



# Cavitation-microstreaming-based lysis and DNA extraction using a laser-machined polycarbonate microfluidic chip

Abdi Mirgissa Kaba<sup>a</sup>, Hyunjin Jeon<sup>a</sup>, Areum Park<sup>b</sup>, Kyungjin Yi<sup>b</sup>, Seonhyeok Baek<sup>a</sup>,  
Aeja Park<sup>b</sup>, Dohyun Kim<sup>a,\*</sup>

<sup>a</sup> Department of Mechanical Engineering, Myongji University, 116 Myongji-ro, Yongin 17058, Republic of Korea

<sup>b</sup> Biomedux, 17 Daehak 4-ro, Suwon 16226, Republic of Korea

## ARTICLE INFO

### Keywords:

Microfluidic nucleic-acid analysis  
Chemical lysis  
DNA extraction  
Micromixing  
Cavitation microstreaming  
Solvent-assisted thermal bonding

## ABSTRACT

We *for the first time* present a microfluidic cavitation-microstreaming-based cell lysis and DNA extraction method. Chemical lysis and DNA extraction have been demonstrated in a microfluidic format but the performance is limited by ineffective mass transport due to low Reynolds number. Here we propose to employ cavitation microstreaming for enhancing chemical lysis and magnetic-bead-based dynamic solid phase extraction (dsPE) of DNA. Cavitation microstreaming condition is optimized by exciting a microfluidic chip at its flexural resonance frequency ( $f_r$ ) measured via electrical impedance spectroscopy. Strong circulatory flows around bubbles excited at  $f_r$  yields vigorous agitation, allowing fast lysis, and DNA extraction and purification. The microfluidic device is rapidly fabricated using CO<sub>2</sub>-laser machining and solvent-assisted thermal bonding of polycarbonate (~25 min). Laser cutting conditions are experimentally determined to achieve a clean sidewall for negligible nonspecific binding and minimal burrs for unobstructed bonding. Solvent exposure and thermal bonding conditions are also experimentally determined for a leakage-free device with excellent dimensional integrity. Our method, although not fully optimized, exhibits an excellent DNA extraction performance, compared to a commercial kit and previous microfluidic methods. High extraction efficiency (76.9 %) and purity (A260/A280 = 1.85) are achieved for a relatively short assay time (~25 min). Notably, DNA from as few as 18 cells is successfully extracted even from a highly diluted cell sample (0.18 cells/μl). PCR and electrophoresis results confirm the excellent quality of the extracted DNA. Considering these notable performances, and straightforward fabrication and operation, we anticipate our DNA extraction method will be widely used in microfluidic nucleic-acid analysis devices.

## 1. Introduction

The global health burden is ever-increasing due to infectious diseases [1,2]. The problem is aggravated by the possible evolutionary potential of certain pathogens and highly-pathogenic viral diseases that could pose significant public health threats (i.e., the recent COVID-19 pandemic) [3,4]. Emerging nucleic-acid-based diagnostics have been important tools to combat such health hazards, as they exhibit high sensitivity, specificity, and the unique potential to detect particular strains of pathogens (e.g., drug-resistant strains) compared to conventional methods that rely on phenotypic expression of antigens or biochemical products [5].

Nucleic acid testing (NAT) for infectious diseases has been traditionally conducted in laboratories equipped with trained professionals and expensive instruments [6]. The recent emergence of rapid, accurate,

portable, and affordable, point-of-care (POC) devices have paved the way for the development of various POC NAT systems [7]. Many POC NAT devices perform nucleic-acid analysis in miniaturized fluidic platforms [8]. Commercialized POC NAT systems including GeneXpert (Cepheid) and FilmArray Torch (BioFire Diagnostics) are good examples [7,8]. These platforms are called microfluidic devices or lab-on-a-chips (LOC). Integrated with microscale channels and chambers, they can manipulate minuscule volumes of liquids [9,10]. These devices promise to perform an entire analytical process encompassing sample preparation, reaction, separation, and detection. However, sample preparation, the primary yet most important step in the NAT, has been consistently referred to as one of the major difficulties in the development of microfluidic POC NAT due to the unique challenges in translating the conventional methods to the microscale [11,12]. The sample preparation includes cell lysis, and subsequent extraction and purification of

\* Corresponding author.

E-mail address: [dohyun.kim@mju.ac.kr](mailto:dohyun.kim@mju.ac.kr) (D. Kim).

<https://doi.org/10.1016/j.snb.2021.130511>

Received 15 April 2021; Received in revised form 4 July 2021; Accepted 26 July 2021

Available online 29 July 2021

0925-4005/© 2021 Elsevier B.V. All rights reserved.

nucleic acid (NA) from the lysate [13].

Cell lysis demonstrated in microfluidic format includes mechanical, laser, thermal, electrical, and chemical methods [14,15]. Compressive or frictional forces physically disrupt the cell membrane in mechanical lysis [16,17]. The mechanical lysis exhibits high lysing efficiency. However, it has significant limitations including complex device fabrication (e.g., nanoknife array [18]), requirement of additional instruments (e.g., motor-controlled rotating external magnet [16]), and difficulty in collecting target biomolecules from lysate (i.e., large and sticky debris) [14,19]. In laser lysis, the expansion and collapse of cavitation bubbles produced by short-pulsed laser cause cells to rupture [20]. The capability of selectively lysing target cells without disrupting nearby cells can be advantageous in certain applications. However, it has significant drawbacks including inapplicability to unsettled cell suspensions [21], expensive optical instrumentation (e.g., Nd: YAG laser) [20], and incompatibility with shock-absorbing substrates like PDMS [22]. In thermal lysis, heat is used to denature proteins in cell membranes and to access cell contents [23]. Microfluidic thermal lysis requires small power due to the reduced heat capacity of a minute sample volume [15]. However, it has disadvantages including difficulty in applying to large-volume samples and continuous-flow lysis [14], and complex microfabrication (e.g., integration of resistive microheaters [23]). Electrical lysis (i.e., electroporation) is used to create pores through the cell membrane that release genetic materials [24]. AC [25] and DC voltages [26], and voltage pulses [27] have been used for lysis. Membrane selectivity (i.e., leaving intracellular-organelle membranes undamaged) [28] can be taken as a unique advantage. However, difficulty in finding optimal voltage signals [29], heat generation and bubble formation [14], and short electrode lifetime have been described as major drawbacks.

Chemical lysis employs surfactant (e.g., SDS, Triton X-100) for solubilization of lipids and proteins in the cell membrane, enzyme (e.g., Proteinase K) for digesting proteins, and chaotropic agents (e.g., guanidine HCl, guanidine thiocyanate) for denaturing proteins and creating hydrophobic environment which accelerates binding to silica surfaces. Various combinations of these reagents were used on trade-offs between assay complexity and lysis efficiency: surfactant only [30], surfactant with enzyme [31], and surfactant with both enzyme and chaotropic agents [32,33]. Enzyme Proteinase K and chaotropic agents are used together in standard benchtop NA extraction kits due to high lysis efficiency [34]. Lysing reagents sometimes inhibit downstream processes [29]. However, the chemical lysis is deemed suitable for microfluidic applications due to straightforward implementation (i.e., mixing with lysing agents), simple microfabrication (i.e., microchamber and microchannels for containing and delivering reagents), and well-established standard reagents from commercial sources [35]. In this work, we opted for chemical lysis to synergistically combine its proven performance in delivering high-quality DNA [36] using widely-available standard reagents and effective mass transport facilitated by cavitation microstreaming.

After lysis, released DNA is extracted and purified. The two most common methods are “static” solid-phase extraction (SPE) and dynamic solid-phase extraction (dSPE) [37]. In SPE, a stationary silica surface is used to capture DNA from mobile lysate [38]. However, fabrication of high-surface-area silica microstructures [39] or reproducible packing of silica microbeads is challenging in a microfluidic format [40]. In dSPE, mobile silica-coated magnetic beads are used to collect DNA in stationary or moving lysate [37,41]. Effective mixing is critical for dSPE for increased interaction between the DNA and bead (i.e., reduced diffusion length), enhancing DNA collection [32]. The DNA-bound beads are later collected by an external magnet. In both techniques, once DNA is attached to the silica surface, a series of purification steps are required to remove unneeded intracellular materials including RNA, protein, and lipids before releasing the DNA for elution [42]. We opted for the dSPE due to the following attributes: 1) proven performance, 2) simple fabrication (no need for silica-bead packing or silica-microstructure

generation), 3) easy replenishing of DNA-binding surface (i.e., bead replacement), 4) flexibility of choosing binding surface (i.e., bead type, size, and concentration), and 5) availability of well-controlled commercial product [32].

In addition to the DNA collection, the entire process of cell lysis, DNA extraction, purification, and elution can be facilitated by effective mixing [34]. However, convective mixing is uniquely challenging in microfluidic devices due to low Reynolds number [43,44]. Various types of microfluidic mixing techniques have been studied for the analysis of biological/chemical targets over the past few decades [45]. One of the two major types of mixing, passive mixing takes advantage of geometrical effects in generating chaotic advection and fast diffusion between thinned fluid laminae with increased contact area [46]. However, the passive mixing generally lacks control (i.e., no adjusting the level of mixing or halting mid-operation) [44]. Moreover, it requires complex microfabrication processes to build special geometries [47]. Regardless, various passive mixing techniques were employed for cell lysis, DNA extraction, and purification [39,48,49].

Active mixing uses external energy sources to disturb fluids, increase the contact area or induce chaotic advection, which eventually enhances mass transport [43,44]. Using external perturbation (e.g., acoustic [50], pressure [51], magnetic [52], thermal [53], or dielectrophoretic [54]) is advantageous as it enables an operational control of mixing [50]. Because cell lysis and DNA extraction consist of multiple steps requiring different extent and time of agitation, the control of mixing is essential [37,41]. Among the various active types, acoustic micromixing has caught much attention due to its affordable and simple device fabrication, and straightforward implementation [55,56], which are qualities useful in microfluidic cell lysis and DNA extraction for POC NAT.

Acoustic mixing employs the streaming of fluid around a surface oscillating at its resonance [50,57]. Highly cited micromixers relied on an acoustic phenomenon called cavitation microstreaming [50,58,59]. As an air bubble trapped in a liquid medium vibrates under an acoustic field, frictional forces created at the air-liquid interface generate a circulatory bulk flow [58]. Cavitation microstreaming exhibits significant advantages including simple activation using an affordable piezoelectric transducer attached to a micromixer [60], a wide range of mixable volume [57], and mixing as fast as 7 ms [50].

In this work, we for the first time propose cavitation-microstreaming-facilitated microfluidic chemical lysis, and silica-magnetic-bead-based DNA extraction and purification. For high-quality DNA extraction with an excellent yield, our method synergistically combines the advantages of cavitation-microstreaming-based effective mixing with the well-established chemical cell lysis and dSPE. Streaming from multiple bubbles trapped in air pockets sweeps the entire mixing chamber for excellent homogenization to enhance mass transport required for chemical lysis and purification. There have been previous attempts to apply cavitation microstreaming to cell lysis without lysing agents [61–63]. However, there is skepticism on whether microstreaming is capable of shearing cells [64]. Moreover, the process has been limited to lysis, and DNA collection has not been demonstrated [63].

Previously, the air bubbles were excited at their theoretically calculated resonance frequency, which was not experimentally validated [50]. Here we excite the air bubbles at the flexural resonance frequency ( $f_r$ ) of the microfluidic device measured using an impedance analyzer to yield more effective mixing [65]. Additionally, a cell-lysis and DNA-extraction protocol suitable for our microfluidic device was developed. The protocol was experimentally evaluated, and its results were compared with those of a commercial kit [41]. Recent work has reported cavitation-microstreaming-based cell-free DNA (cfDNA) extraction [56]. Although the customizable chamber volume (10–1100  $\mu\text{L}$ ) was advocated, a tedious and time-consuming resonance-frequency search based on manual frequency sweeping was required. Furthermore, cell lysis, the most important step in NAT, was not demonstrated.

We relied on laser ablation and solvent-assisted thermal bonding to fabricate our multilayer polymer microfluidic device. Direct writing

using laser ablation is advantageous due to affordability, fast turnaround time, suitable machining precision, and no need for a cleanroom. Instead of PMMA (polymethyl methacrylate), a common thermoplastic for microfluidic devices, we chose polycarbonate (PC) due to its solvent compatibility with our lysis protocol (i.e., ethanol) and optical clarity for assay observation. Thermal bonding has been commonly used for multilayer thermoplastic devices [66]. However, high temperature and pressure could lead to a collapse of microfeatures [67]. Therefore, we opted for solvent-assisted thermal bonding where temperature and pressure requirements were alleviated [68]. Parameters for laser cutting (i.e., power, speed, and frequency) were experimentally determined [69, 70] to achieve 1) smooth surface to minimize sporadic bubble trapping and nonspecific binding of cells and intracellular materials, and 2) minimized burrs for unobstructed bonding of machined layers. Bonding parameters (i.e., solvent-exposure time, substrate-to-solvent distance, bonding time, pressure, and temperature) were also experimentally determined for dimensional integrity and leakage-free bonding [70,71].

The performance of our microfluidic device was thoroughly evaluated using two mammalian cell lines (i.e., K562, CHO-K1). DNA yield, extraction efficiency, and purity were characterized. The quality of the extracted DNA was further established by PCR amplification and gel electrophoresis of a target gene [72]. A parallel experiment was conducted using a commercial DNA-extraction kit to compare and evaluate our device and assay.

## 2. Experimental

### 2.1. Materials and reagents

A transparent 500- $\mu\text{m}$ -thick polycarbonate (PC) sheet was purchased from Wholesale POS (#361507432172, Chelmsford, UK). Commercial DNA-extraction kits, MagaZorb DNA Mini-Prep Kit (based on silica-coated magnetic bead) and QIAamp DNA Mini Kit (based on silica column) were obtained from Promega (#0000397378, Madison, WI, USA) and Qiagen (#157048166, Hilden, Germany), respectively. MagAttract Suspension G magnetic bead (#1026901) was also obtained from Qiagen. DNA-concentrator kit was purchased from Zymo Research (#ZRC204994, Irvine, CA, USA). K562 (human chronic myeloid leukemia cell) and CHO-K1 (Chinese hamster ovary cell) were purchased from the Korean Cell Line Bank (Seoul, South Korea). Phosphate buffered saline (PBS, pH 7.4) and 99.8 % chloroform were obtained from Sigma-Aldrich (St. Louis, MO, USA). 99.9 % ethanol was purchased from Daejung Chemicals and Metals (Shiheung, South Korea).

### 2.2. Microfluidic chip design

The microfluidic chips were designed using AutoCAD (Autodesk, San Rafael, CA, USA). The microfluidic chip consists of three functional layers (Fig. 1a); a top layer with fluidic interfaces, a chamber layer housing a microchamber, and a bottom layer for bonding a piezoelectric transducer (Fig. 1b).

The microchamber is a circular cavity of 17.7 mm in diameter, which is located at the center of the chamber layer, connected to both the inlet and outlet channels (2.75 mm  $\times$  1.5 mm) (Fig. 1c). The circular chamber is surrounded by six air pockets for trapping oscillating bubbles. It is the crucial part of the chip where cell lysis, DNA extraction, and purification are performed. The inlet channel serves as a route for loading the sample (i.e., cell suspension) and reagents (i.e., lysis and purification buffers). Products of sample processing including extracted DNA and unwanted intracellular materials (e.g., RNA, protein, lipids, etc.) are eluted through the outlet channel. Initially, the channel dimension was larger (i.e., 5.5 mm  $\times$  2 mm) adopted from our previous work [65] but this design results in significant unagitated dead volume (20  $\mu\text{L}$ ) affecting DNA-extraction performance. By downsizing inlet/outlet channels, the dead volume was minimized (5  $\mu\text{L}$ ).

The air pockets are cavities of an inverted triangular shape that are

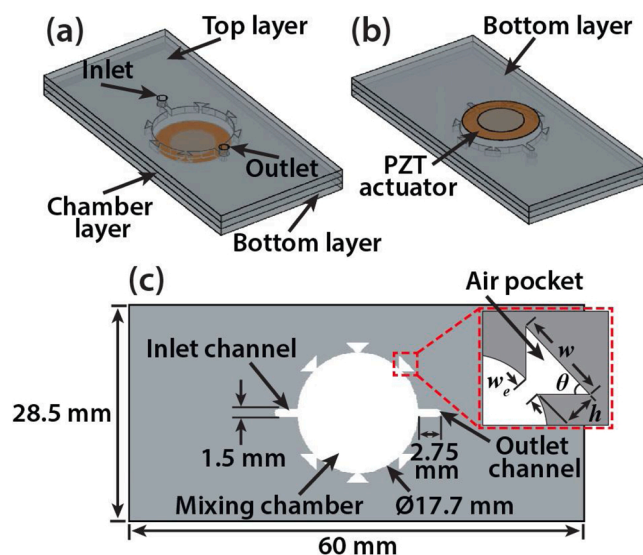


**Fig. 1.** Design of the multilayer microfluidic cell-lysis and DNA-extraction chip. (a) Top layer with an inlet and outlet ports, chamber layer with a microchamber and inlet/outlet channels, and (b) bottom layer with a piezoelectric transducer. (c) The chamber layer has key microfluidic features: a circular microchamber (17.7 mm diameter) and connected inlet and outlet microchannels (2.75 mm  $\times$  1.5 mm). Six inverted-triangular-shaped air pockets (height  $h$ , entrance width  $w_e$ , and entrance angle  $\theta$ ) are evenly distributed on the microchamber perimeter for effective mixing.

positioned on the perimeter of the microchamber at equal distance from one another (Fig. 1c, inset figure). Each air pocket serves as a trap for an air bubble. The shape of the air pocket was determined based on the stability and effectiveness of cavitation microstreaming generated by the trapped bubble [65]. The vibration of the bubbles formed inside the air pockets creates frictional forces at the air-liquid interface that induce the circulatory bulk flow called cavitation microstreaming [50,73]. Therefore, the air-water interface must be stable for long mixing operation and wide for a broad mixing zone swept by streaming. Design parameters of the air pocket that significantly affect the bubble stability and the streaming coverage are entrance width  $w_e$  (i.e., the narrow front section of the pocket) and entrance angle  $\theta$  (i.e., the base angles of the triangle, Fig. 1c). Experimental optimization was conducted to find  $w_e$  that maximizes the bubble stability while maintaining a wide mixing zone. During the optimization process,  $\theta$  was maintained at 45  $^\circ$  according to our previous study [65] (see Section 3.3 for more detail).

### 2.3. Microfluidic-chip fabrication

The microfluidic chip was in-house fabricated using laser machining and solvent-assisted thermal bonding. A CO<sub>2</sub>-laser machine was used to cut PC (polycarbonate) sheets into rectangular layers and to pattern the designed microfluidic features on each layer (Fig. 2a,b). Solvent-assisted thermal bonding was used to permanently bond the three patterned layers (Figs. 2c,d and 3a,b). Once bonded, a piezoelectric transducer was permanently glued to the bottom of the chip.

#### 2.3.1. Laser machining

The PC layers and corresponding microfeatures were cut by a benchtop CO<sub>2</sub>-laser machine (Mini 18, 10.6- $\mu\text{m}$  wavelength, Epilog Laser, Golden, CO, USA; Fig. 2b). Each PC sheet, covered with a clear protective film, was cleaned using disposable wipes (KIMTECH, Kimberly-Clark Professional, Roswell, GA, USA) before machining. The PC sheet was temporarily affixed to a lifting frame made of PMMA (60 mm  $\times$  90 mm, 5-mm thick) using a double-sided tape. The lifting frame carrying the PC sheet was placed on the honeycomb grid (Fig. 2b, inset figure) so that the sheet was lifted about 5.6 mm above the grid to

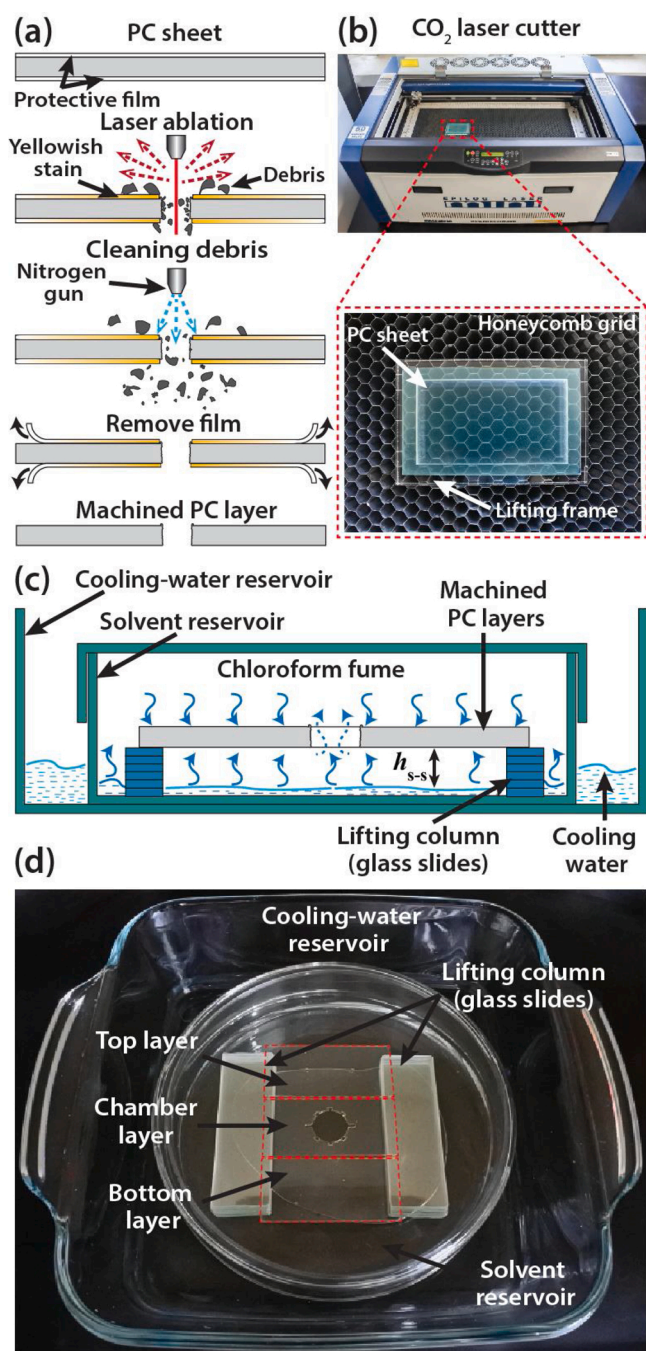


**Fig. 2.** Laser-micromachining and solvent-treatment processes. (a) Process flow of laser micromachining. A 500- $\mu\text{m}$ -thick PC sheet covered with a protective film was cut through using an optimized laser machining condition to form three layers (top, chamber, and bottom; Fig. 1a) and their corresponding microfluidic features. After machining, pressurized nitrogen gas was used to clean laser-ablation debris, and later the protective film was removed to reduce yellowish stain around cut surfaces. (b) Laser machining setup. A custom-made PMMA lifting frame on the honeycomb grid was used to lift the PC sheet to minimize burning marks. (c) Schematic and (d) photograph of the solvent-treatment setup. Thoroughly cleaned PC layers were suspended at the predetermined substrate-to-solvent height  $h_{s-s}$  on the two lifting columns inside an enclosed glass petri dish containing chloroform. The petri dish was placed inside a large glass-drying dish containing a cold-water bath for cooling.

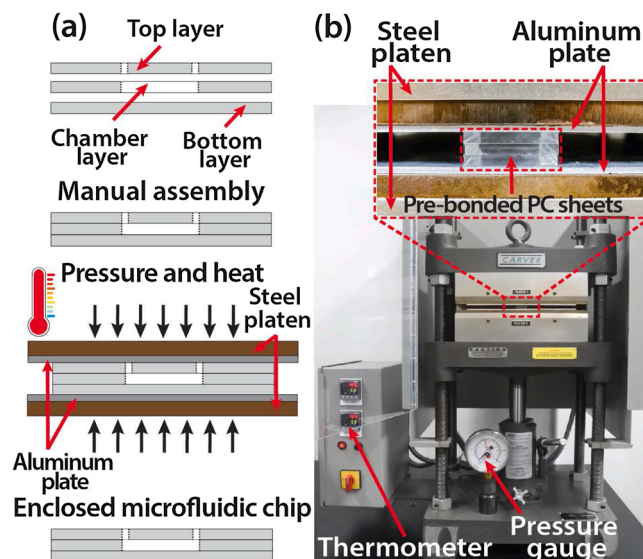


**Fig. 3.** Thermal-bonding process. (a) Three solvent-treated PC layers were manually aligned and temporarily assembled. Then the assembly was pressed at predetermined bonding temperature  $T_b$ , pressure  $P_b$ , and time  $t_b$  to obtain a tightly enclosed microfluidic chip with excellent structural integrity. (b) A bench-top hot press with temperature control was used for bonding. The assembly was interposed between two Teflon-covered aluminum plates to prevent the PC from sticking to the steel plates. Note: thicker (5 mm) PMMA pieces were shown in the inset image for visualization purpose.

prevent burning marks. Experimentally determined laser cutting conditions were used to pattern microfeatures with smooth cut sidewalls to reduce nonspecific biomolecular adsorption and sporadic bubble trapping. In this way, burrs, ridge-shaped waveform of solidified molten PC along the edge of the cut, were also minimized to obtain well-sealed (i.e., leakage-free) microfluidic chips (see Section 3.1). Pressurized nitrogen gas (Yongin Gas, Yongin, South Korea) was used to clean debris (i.e., solidified molten PC particulates ejected and scattered) from the cut surfaces (Fig. 2a). Yellowish stain from the vaporized PC is also a usual occurrence during laser cutting. For a simple remedy, the protective film was remained unpeeled on the PC layers during laser cutting. The stained film was peeled off afterward to minimize staining on the cut surfaces. An upright microscope (BX-40, Olympus) and image-analysis software (ImageJ, NIH, Bethesda, MD, USA) were used for visual observation and evaluation of micromachining results.

### 2.3.2. Solvent treatment

Chloroform was poured into a petri dish containing two stacks of microscope slides (#7101, Ehwa Glass, Shanghai, China) serving as lifting columns (Fig. 2c,d). The petri dish was placed inside a large glass-drying dish with a cold-water bath for cooling during solvent exposure [74]. Each machined PC layer was carefully placed on the two lifting columns for suspending above a pool of chloroform. The solvent reservoir was covered with a lid to minimize chloroform-vapor leakage and to increase its efficacy. Upon exposure to chloroform, a thin swollen solvent-saturated region of the PC layer with increased polymer chain movement is formed. When brought in contact with a similarly-treated PC layer, interchain entanglement occurs, leading to bonding of the two surfaces [74]. However, when the PC layer is overexposed to the solvent fume, deformation of patterned microfeatures or melting of the whole layer could result. Thus, process parameters for the solvent exposure, namely exposure time ( $t_e$ ) and substrate-to-solvent distance ( $h_{s-s}$ ) were experimentally optimized to find a bonding condition for a leakage-free and minimally deformed microfluidic chip.

### 2.3.3. Thermal bonding

The surface of the PC layers turned adhesive after solvent treatment. The three layers were manually aligned and temporarily attached to one another (Fig. 3a). These pre-bonded PC layers were subsequently placed inside a bench-top hot press with temperature control (Model 4122, Carver, Wabash, IN, USA; Fig. 3b) for permanent bonding. The steel platens were preheated to 125 °C to guarantee rapid heat transfer. Thin aluminum plates (250 mm × 250 mm, 2-mm thick) covered by a Teflon film (#ASK013AD, Alphaflon Teflon specialist, Seoul, South Korea) were interposed between the steel platens and PC layers to prevent stiction.

In conventional thermal bonding, the PC layers are heated to a temperature near or above their  $T_g$  (glass transition temperature), and enough pressure is applied to ensure a strong bond. Exposing PC layers to chloroform before the bonding process turns the surface adhesive and lowers  $T_g$ , effectively reducing the bonding temperature ( $T_b$ ), pressure ( $P_b$ ), and time ( $t_b$ ) [70]. On the other hand, too much temperature, pressure, and time may lead to a reduction of microfluidic features (i.e., chamber and channels) or in severe cases, a collapse of an entire microfluidic chip. To fabricate a firmly-enclosed chip with excellent structural integrity, the bonding parameters, namely  $T_b$ ,  $P_b$ , and  $t_b$ , were experimentally determined.

### 2.3.4. Bottom-layer coloring and PZT-transducer bonding

A PZT (lead zirconate titanate) transducer (7BB-15-6L0, Murata, Kyoto, Japan) was bonded to the PC bottom layer (Fig. 1b) to excite trapped bubbles. This piezoelectric transducer is a so-called disc bender, built from a PZT ceramic (0.1 mm thick and 10 mm diameter) bonded to a thin brass disc (0.1 mm thick and 15 mm diameter). Its resonance frequency in the specification was  $6.0 \pm 1.0$  kHz.

We noticed that a strong yellowish reflection from the brass plate of the PZT transducer through the transparent bottom layer hinders clear observation. To alleviate this problem, the bottom was rendered opaque by spray painting before attachment of the PZT transducer. White spray paint (Dupli-color, Motip Dupli, Hassmersheim, Germany) was chosen because high-contrast imaging using seeded black magnetic beads was possible for streaming visualization (Section 3.1.2). Once the paint dries, the PZT transducer was permanently bonded to the center of the bottom layer using a superglue (Loctite 401, Henkel, Dusseldorf, Germany).

## 2.4. Design and fabrication of a magnet jig

For smooth assay operation and facile imaging of cell lysis and DNA extraction, a jig that can carry the microfluidic chip, termed as a magnet jig, was designed and fabricated (Fig. 4). The jig has a horizontal platform having vertically positioned chip slots on both ends. The slots were used to firmly accommodate and readily release the microfluidic chip on

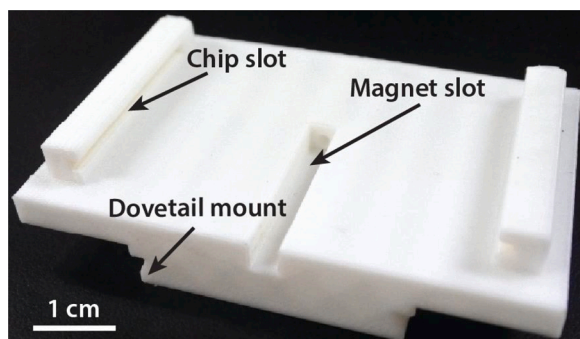


Fig. 4. Custom-made “magnet jig”. The chip slots on both sides of the jig were used to secure the microfluidic chip during experiments. The magnet slot carries a permanent magnet that can be readily mounted and dismounted on demand. The dovetail mount allows easy coupling and decoupling of the jig to a custom-built XY translational stage.

demand. A slot for a permanent magnet was embedded in the platform, stretching across the center. This slot was designed to insert or remove a permanent magnet for collecting or releasing magnetic beads inside the microchamber. The bottom of the jig has a so-called dovetail mount for quick coupling to a custom-built XY translational stage (see Section 2.6). The jig was designed using AutoCAD and fabricated using a 3D printer (3DWOX, Sindoh, Seoul, South Korea).

## 2.5. Electrical-impedance-based determination of resonance frequency

The piezoelectric transducer vibrates with maximum amplitude at its resonance frequency ( $f_r$ ), efficiently converting input electrical energy into output mechanical bending [75]. At this resonance frequency, the electrical impedance of the piezoelectric device becomes minimum, and this phenomenon is called “resonance”. Then a local maximum of the impedance follows at a higher frequency, which is called “anti-resonance”. A local maximum of phase angle  $\theta$  appears between the resonance and anti-resonance frequencies. Locating this “impedance signature” allows accurate determination of  $f_r$  (i.e., frequency of a “resonance” peak). A microfluidic chip (essentially a mechanical structure) bonded with a piezoelectric device exhibited similar impedance signatures [65]. Thus, an impedance analyzer (MFIA, Zurich Instruments, Zurich, Switzerland) was used to locate the resonance signatures of the microfluidic chip bonded with a piezoelectric transducer (Fig. 5). Among resonance signatures appeared in a specified frequency range, the “strongest” signature (i.e., the maximum magnitude difference between the resonance and anti-resonance  $\Delta|Z|$  and the highest phase peak  $\Delta\theta$ ) was sought. Then  $f_r$  of the strongest signature was determined and used to excite the microfluidic chip for maximum bubble oscillation.

A sinusoidal signal of 12 V<sub>p-p</sub> with frequency ranging from 1 kHz to 10 kHz was applied to a microfluidic device using the impedance analyzer. An instrument-control software (LabOne, Zurich Instruments) was used to measure magnitude  $|Z|$  and phase angle  $\theta$  of impedance across the specified frequency range. Initially,  $f_r$  of the PZT transducer, provided in the manufacturer’s specification, was confirmed by locating the strongest resonance signature. Then,  $f_r$  of the microfluidic chip bonded with this PZT transducer was found. In order to mimic the mechanical conditions during cell-lysis and DNA-extraction experiments,

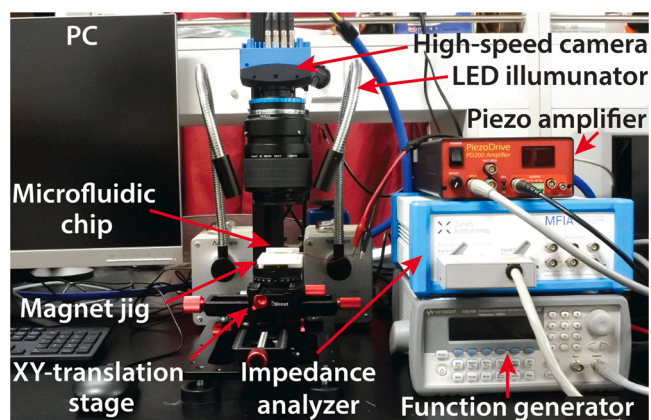


Fig. 5. Experimental setup for impedance measurement and high-speed flow visualization. An impedance analyzer was used to measure the electrical impedance of the microfluidic chip. Through the strong electromechanical coupling between the microfluidic chip and the attached PZT transducer, the flexural resonance frequency of the chip can be determined based on the measured impedance information. A function generator and piezo amplifier were used to excite the microfluidic chip with 60 V<sub>p-p</sub> at the determined resonance frequency. A high-speed camera equipped with a macro lens was used to observe streaming patterns and monitor mixing processes inside the microchamber. LED light sources assisted with imaging. A custom XY stage was built to carry and maneuver the chip-mounted magnet jig.

the microfluidic chip was filled with liquid (i.e., PBS buffer), and the fluidic ports were sealed using a Teflon tape during the measurement.

## 2.6. High-speed imaging for assay observation

The microfluidic chip was mounted on the magnet jig, which was then coupled to a custom-built XY translational stage (Fig. 5). The stage allows rotational and X-Y translational motion of the chip-mounted jig, and vertical movement for the camera. The high-speed camera (EoSens 4CXP, Mikrotron, Bavaria, Germany) used in this work has a capacity of capturing a maximum of 563 frames per second at a resolution of  $2336 \times 1728$ . The camera was fitted with a macro zoom lens (MP-E 65 mm F/2.8 1-5 $\times$ , Canon, Tokyo, Japan) for monitoring the microchamber and observing streaming patterns around the trapped bubbles. Two fiber-optic LED light sources (LED-50W, AmScope, Irvine, CA, USA) were used for illumination during imaging.

A function generator (33210A, Keysight Technologies, Santa Rosa, CA, USA) was used to generate a  $3 V_{p-p}$  sinusoidal signal that was amplified to  $60 V_{p-p}$  by a piezo amplifier (PD 200, PiezoDrive, Newcastle, Australia). The amplified signal was used to excite the microfluidic chip at its determined resonance frequency for mixing. Black silica-coated magnetic beads on the white background (i.e., bottom layer) allowed high-contrast observation of mixing processes.

## 2.7. Cell-lysis and DNA-extraction procedure

We performed cell lysis and subsequent DNA extraction using the fabricated microfluidic chip and subsequently a commercial kit as a control. A new experimental protocol for our microfluidic chip was devised to accommodate for a different container geometry and fluid-dynamic condition (i.e., flat microchamber of 100  $\mu\text{L}$  volume vs. microcentrifuge tube of 1500  $\mu\text{L}$  volume) by modifying a standard protocol of magnetic-bead-based commercial kit (MagAttract HMW DNA kit). The K562 and CHO-K1 cell lines were tested for evaluation of our device and protocol.

### 2.7.1. Cell preparation and count

K562 cells (Korean Cell Line Bank) were grown by our collaborator (Biomedux, Suwon, South Korea). Once harvested, the cells were washed using  $1 \times$  PBS buffer and resuspended in fresh culture media RPMI 1640 (Thermo Fisher, Waltham, MA, USA). CHO-K1 cell samples were prepared after received from Korean Cell Line Bank without in-house culture. The cells, initially attached to a T25 flask, were washed using  $1 \times$  PBS after the culture media was aspirated. Subsequently,  $1 \times$  Trypsin EDTA (Thermo Fisher) was loaded into the flask and incubated for 10 min to detach the cells from the bottom surface. The detached cells were later aspirated, and the solution was centrifuged. The cell pellets were resuspended in a fresh RPMI 1640 media for counting.

Cells were counted manually using a disposable hemocytometer (C-Chip DHC-N01, INCYTO, Cheonan, South Korea). An inverted microscope (IX-70, Olympus) fitted with an sCMOS camera (Zyla 5.5, Andor Technology, Belfast, UK) was used to image cells suspended inside the hemocytometer. The cells in the images were counted using Multi-point tool of ImageJ. Theoretical and experimental details for cell counting are given in Section S.1 of Supplementary Information (SI).

### 2.7.2. Microfluidic cell-lysis and DNA-extraction workflow

Before using the microfluidic chip, we ran a few test experiments of cell lysis and DNA extraction at “macroscale” (i.e., in a microcentrifuge tube) using reagents (i.e., lysis buffer, washing buffers, and elution buffer) from QIAamp DNA Mini Kit and a magnetic bead (MagAttract Suspension G). We adopted an experimental protocol of MagAttract HMW DNA kit provided by Biomedux. The reagents from QIAamp DNA Mini Kit and magnetic bead were selected on account of their proven performance in DNA extraction [33,76]. After confirming that the macroscale lysis and DNA extraction work properly, we modified the

protocol to be compatible with our microfluidic chip. For example, sample and reagent volumes were scaled down to fit inside the microchamber of a smaller volume (100  $\mu\text{L}$  vs. 1500  $\mu\text{L}$ ), and special loading and aspiration techniques for the microfluidic chip were devised to ensure the absence of unnecessary bubbles. The assay workflow is as follows. The detailed protocol is described in Section S.2 (SI).

#### Step 1: chip preparation

The microfluidic chip is tightly affixed onto the magnet jig (the chip is mounted in the jig throughout all assay steps). Then the microchamber and microchannels are thoroughly washed using  $1 \times$  PBS for 1 min (i.e., for a new chip) or ethanol for 0.5 min (i.e., for a used chip) as seen in Fig. 6a. A micropipette is used for loading and aspirating fluids from the microchamber through the entire assay steps.

#### Step 2: lysis-mixture loading

A 37- $\mu\text{L}$  solution of ethanol and magnetic beads is injected into the microchamber followed by a 63- $\mu\text{L}$  mixture of cells, lysis buffer, and Proteinase K (Fig. 6b). Once the two mixtures are loaded successively into the chip, the inlet and outlet ports are sealed by a Teflon tape (#AG021AD, Alphaflon Teflon specialist) to prevent leakage in the following steps. During loading, the microfluidic chip is tilted, so that the inlet port is situated lower than the outlet port. Then, the two mixtures were loaded through the inlet port using a micropipette and filled the microchamber sequentially from the bottom edge to the top edge against gravity, with caution not to create bubbles (i.e., bubbles could form from unwetted region and/or corner flow). Bubble formation was also avoided by swaying the chip left or right during loading, to direct liquid towards the said region. This technique helped smooth the loading of liquid without bubble formation and was applied throughout the protocol in steps where loading takes place (see Section 3.4)

#### Step 3: cell lysis

The consecutively loaded liquids in the microchamber are mixed for cell lysis using cavitation microstreaming (Fig. 6c). As the cells break open, DNA and other intracellular materials are released. DNA is selectively attached to the magnetic beads due to molecular interaction (i.e., weak electrostatic repulsion forces, dehydration, and hydrogen-bond formation) under high-ionic-strength chaotropic conditions [77].

#### Step 4: bead collection and removal of intracellular materials

A rectangular neodymium magnet was circled above the microchamber in a spiral motion to drag suspended beads into a loose aggregate at the center. Then the same magnet is inserted below the chamber (i.e., in the magnet jig). In this way, DNA-bound magnetic beads are collected at the edge of the chamber as a compact aggregate (Fig. 6d). Once the magnetic beads are collected, the Teflon tape was removed, and the liquid containing all unnecessary materials is eluted for disposal. The chip is held at an angle and swayed in a similar manner as described in Step 2 to elute waste without remnant liquid inside the chamber.

#### Step 5: purification

A 100- $\mu\text{L}$  of first washing buffer is loaded into the microchamber while the aggregate of DNA-bound magnetic beads is still at the edge. Next, the inlet and outlet ports are closed with the Teflon tape, the magnet is removed from the jig, and the chip is excited. Mixing facilitates suspension of remaining unnecessary intracellular materials in washing buffer while the DNA remains at the bead surface (Fig. 6e). After thorough mixing, magnetic beads are collected in the same manner as done in Step 4, the Teflon tapes are removed, and the washing buffer is eluted for disposal (Fig. 6f). This step is repeated once more with a second washing buffer of the same volume.

#### Step 6: DNA elution

A 100- $\mu\text{L}$  of elution buffer (i.e., a low-ionic-strength solution for detaching the DNA [15]) is loaded into the microchamber with the aggregate of DNA-bound beads still in place. Ports are covered with Teflon tape, and the magnet is removed. The chip is agitated to detach DNA from the bead surface and to suspend it in the elution buffer (Fig. 6g). Finally, the magnetic beads are collected, the tapes are removed, and the buffer containing the DNA is eluted for collection

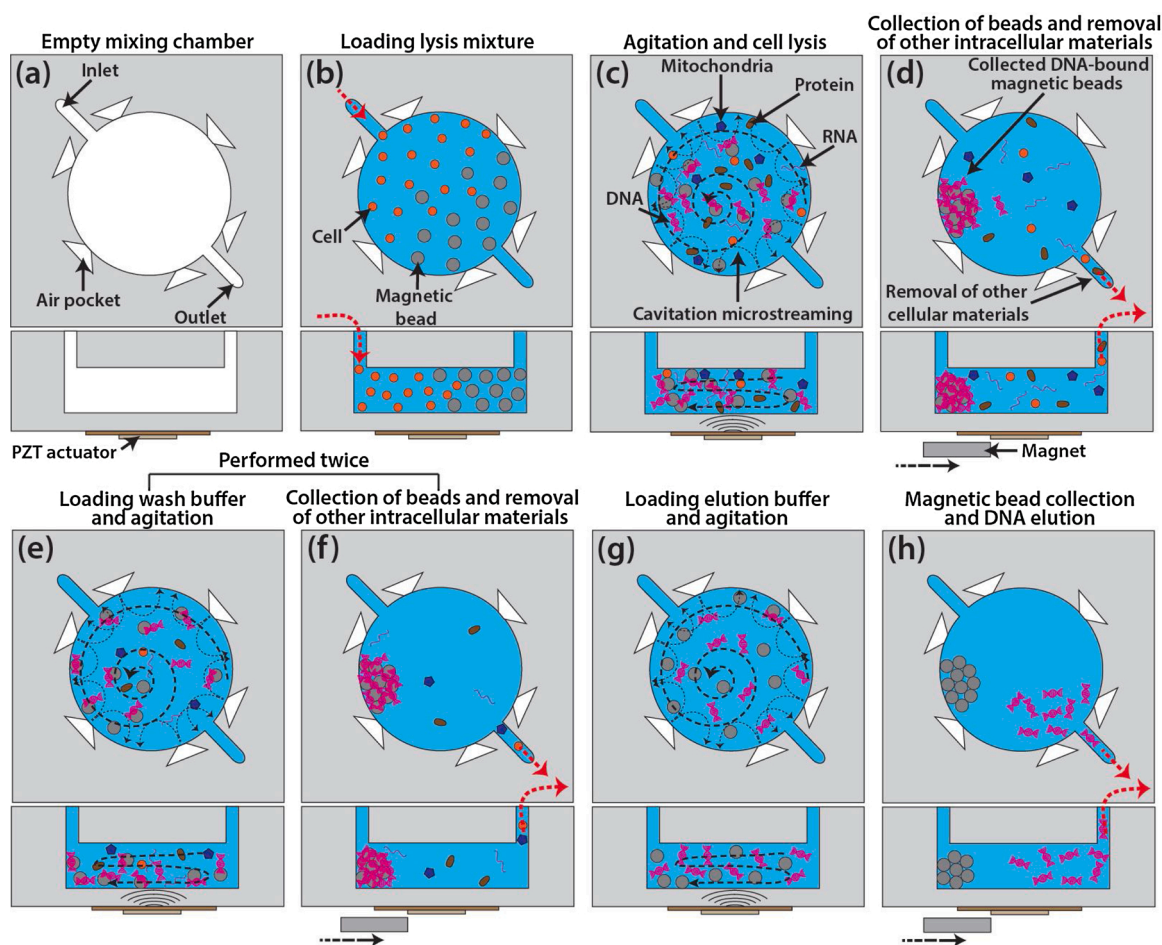


**Fig. 6.** Workflow of microfluidic cell lysis and DNA extraction. A top view (top row) and side view (bottom row) of the microchamber are shown for each step. **Step 1.** (a) The microchamber and microchannels are thoroughly cleaned. **Step 2.** (b) Magnetic beads mixed with ethanol are loaded into the chamber, followed by a mixture containing cells, lysis buffer, and Proteinase K. **Step 3.** (c) The chip is excited at its resonance frequency by the bonded PZT actuator, generating agitation. DNA and intracellular materials are released from lysed cells. DNA is attached to the silica-coated magnetic beads. **Step 4.** (d) Just before the PZT transducer is turned off, a permanent magnet is circled above the chamber in a spiral motion to collect suspended beads into a loose aggregate. Then the same magnet is inserted below the chamber to collect the beads into a compact aggregate to an edge of the chamber. The processed liquid containing interfering intracellular materials is removed. **Step 5.** (e) A first washing buffer is loaded, and the chip is agitated. (f) DNA-bound magnetic beads are collected, and remaining undesirable intracellular materials (i. e., waste) are removed. (e) and (f) are repeated once with a second washing buffer. **Step 6.** (g) An elution buffer is loaded, and the chip is agitated. DNA is detached from the silica-coated magnetic beads and released into the buffer. (h) Magnetic beads are collected, and DNA is eluted for collection.

(Fig. 6h).

### 2.7.3. Cell lysis and DNA extraction using a commercial kit

A control experiment was conducted using a commercial magnetic-bead-based DNA-extraction kit (MagaZorb DNA Mini-Prep kit). We modified the manufacturer's protocol, specifically the collection time of DNA-bound beads. We observed a significant loss of DNA if beads were collected for 1.5 min as per the manufacturer's protocol. After several attempts, we were able to minimize DNA losses by collecting beads for 4 min. The final protocol for the commercial kit is described in detail in Section S.3 (SI).

## 2.8. Performance analysis of the microfluidic cell lysis and DNA extraction

Extraction efficiency is an important figure of merit that can gauge DNA extraction performance regardless of extraction methods, sample volume, or concentration. First, we characterized the concentration of DNA extracted using our microfluidic chip. The concentration was later used in calculating extraction efficiency. The purity of the DNA was also

measured to examine its potential for downstream processes. We also conducted PCR amplification and gel electrophoresis to validate the quality of the extracted DNA. The dynamic range and limit of extraction (LOE) of our device was also evaluated to examine its operational domain and applicability to a scarce amount of cells. The results were compared with those from the commercial kit to validate our microfluidic device and protocol.

### 2.8.1. Characterization of concentration, extraction efficiency, and purity

A UV/Vis spectrophotometer (NanoPhotometer-P330, Implen, Bayern, Germany) was used for characterization of concentration, extraction efficiency and purity. The theoretical detail is given in Section S.4 of SI. The concentration of extracted DNA was measured using a well-established UV-absorbance technique at a wavelength of 260 nm (i. e., A<sub>260</sub>) and adjusted for turbidity measured at A<sub>320</sub> [78].

The extraction efficiency is defined as the ratio of the amount of extracted DNA to the loaded amount. The loaded amount was calculated from measured cell count (Eq. S-1 in SI) multiplied by DNA mass of a single cell [33]:

$$\text{Extraction efficiency (\%)} = \frac{\text{Extracted DNA mass (ng)}}{\text{number of loaded cells} \times \text{average DNA mass of a single cell (ng)}} \quad (1)$$

The purity of extracted DNA, an indicator of its suitability for downstream processes, was also determined using A260 and A280 values (Eq. S-4 in SI) [41].

### 2.8.2. PCR amplification

In addition to the spectrophotometric purity characterization, the quality of the DNA extracted using both the microfluidic device and the commercial kit was characterized using PCR in our collaborator's laboratory (Biomedux). PCR is a robust quality-determining technique based on selective amplification of a segment of "pure" DNA. A 116-bp von-Willebrand-factor (vWF) gene was amplified using a thermocycler (SimpliAmp Thermal Cycler, ThermoFisher, Waltham, MA, USA). A 20  $\mu\text{L}$  of PCR-reaction mixture consisted of 0.0125 mM primers (1  $\mu\text{L}$ ), 2  $\times$  DNA free-HotTaq PCR master mix (10  $\mu\text{L}$ ; CellSafe, Yongin, South Korea), a DNA sample (3  $\mu\text{L}$ ), and DI water (5  $\mu\text{L}$ ) was loaded for thermal cycling. The primers were designed by the Biomedux:



The first amplification cycle consisted of a denaturation process at 95  $^{\circ}\text{C}$  for 5 min, an annealing process at 55  $^{\circ}\text{C}$  for 30 s, and an extension process at 72  $^{\circ}\text{C}$  for 1 min. The remaining 35 cycles followed the same procedure except that each denaturation step was performed for 30 s, and the last extension process was run for 5 min.

### 2.8.3. Gel electrophoresis

Electrophoresis was performed using 2% agarose gel made in house for end-point detection of PCR products. The running condition was 250 V for 25 min. After the completion of electrophoresis, the gel was stained using the Dyne loading star dye (#A751, Dyne Bio, Seongnam, South Korea) according to the manufacturer's protocol. PCR products were then identified using a custom-built gel-documentation system (Biomedux). More detail on gel electrophoresis is given in Section S.5 of SI.

### 2.8.4. Evaluation of dynamic range and lower limit of extraction

The dynamic range and limit of extraction (LOE) of our device were examined using K562 cells to check its working range and applicability for a scarce amount of cells, respectively. Samples of a range of cell numbers spanning five orders of magnitude ( $1.8 \times 10^1$ – $1.8 \times 10^5$ ) were prepared by serial dilution in 100- $\mu\text{L}$  aliquots. DNA was extracted from each aliquot and concentrated using a spin column (ZYMO Research) before PCR. The spin column's manufacturer protocol was modified to concentrate the DNA effectively. The DNA was concentrated to enhance the limit of end-point electrophoresis detection of PCR products from a small number of cells ( $1.8 \times 10^1$ – $1.8 \times 10^3$ ). The amplification cycle and DNA sample volume were also increased to 40 cycles and 6  $\mu\text{L}$  respectively, for the same reason. The smallest number of cells detected by PCR and gel electrophoresis was considered as the LOE.

## 3. Results and discussion

### 3.1. Experimental determination of microfabrication condition

#### 3.1.1. Determination of laser-machining parameters

A  $\text{CO}_2$ -laser machining is well known for its suitability in providing quick and affordable machining of thermoplastic substrates for microfluidic devices [79]. As the laser beam interacts with polymer, a

substantial amount of thermal energy gets absorbed, which causes melting and vaporization of the polymer. A high-pressure gas blown at the cut surface helps to remove debris [80]. The remaining burrs can prevent effective sealing during bonding, leading to leakage. In addition, a rough sidewall of the cut may cause nonspecific entrapment of biomolecules and sporadic attachment of bubbles.

PC (polycarbonate) is a substrate suitable for microfluidic devices handling mild solvents including methanol and ethanol [81] and in relatively high-temperature conditions (i.e.,  $T_g = 147$   $^{\circ}\text{C}$  vs. 105  $^{\circ}\text{C}$  of PMMA) [82]. In addition, its biocompatibility has been appreciated in the bioscience community (e.g., petri dish, cell-culture flask). We choose the PC as the substrate material because ethanol is used during the lysis step (Section 2.7.2), and biological components including cells and DNA are processed inside the microfluidic device. However, PC has been known to exhibit pronounced burrs and surface roughness during laser machining compared to other popular thermoplastics including COC (cyclic olefin copolymer) and PMMA [69,83,84]. Consequently, we sought to optimize laser-cutting parameters, namely power (P, %), speed (S, %), and frequency (F, Hz) to minimize these machining artifacts [79].

The cutting parameters of our laser machine were tested by making a 10-mm straight incision on a 500- $\mu\text{m}$ -thick PC sheet (Fig. 7a) in a range of P = 2–6% (100% = 30 W), S = 1–5% (100% = 93.5 mm/s), and F = 2750–5000 Hz (maximum 5000 Hz). We noted that an increase in P leads to an increase in kerf (i.e., cut) width [69,83]. An increase in S consistently generated less burr [84] while an increase in F improved the surface roughness of cut sidewalls [69]. Thus, F was fixed to the maximum value of 5000 Hz while experimentally investigating the remaining parameter combinations of P and S. As the PC sheet cannot be cut at excessively low P (2–3%) and high S (4–5%), these combinations were discarded. We also circumvented combinations P = 2–4% and S = 1–3% that created substantial blisters and/or corrugated burr (Fig. 7a). From the remaining set of combinations, we found the one that cut through the PC sheet (i.e., complete penetration) with the least corrugated burrs and smoothest sidewall surfaces: P = 6%, S = 3%, and F = 5000 Hz. As shown in Fig. 7a (top), an unoptimized laser-cutting condition (P = 3%, S = 1%, F = 5000 Hz) generated significantly large, corrugated burrs and distinctly blistered (radius  $\sim$  2–15  $\mu\text{m}$ ) sidewall surfaces. Fig. 7a (bottom) shows a stark difference in the machining quality obtained using the optimized condition with noticeably reduced burrs and smooth sidewall surfaces.

The PC has been known to catch fire, discolor (i.e., dark yellowish stain), and generate a scorching smell during laser cutting [85]. Generated di(2-ethylhexyl) phthalate may pose a health risk to the operator [86]. Necessary cautionary measures (i.e., proper ventilation/filtration system, wearing gas masks and gloves) were taken to avoid exposure to the hazardous vapor. We observed that yellowish stain caused by the fume discolored the PC workpiece, causing a permanent reduction in transparency (Fig. S1 of Section S.6 in SI); it was difficult to observe assay through a discolored PC layer. Therefore, we devised a simple remedy for the staining problem. The protective plastic films on both sides of the PC sheet were unpeeled during the laser machining process (Fig. 2a). Removing the films after cutting significantly helped in obtaining clear PC layers.

#### 3.1.2. Determination of solvent-treatment and thermal-bonding parameters

The parameters, solvent-exposure time ( $t_e = 0.5$ –40 min), and substrate-to-solvent distance ( $h_{s-s} = 5$ –13 mm) were experimentally examined for fine-tuning of the solvent-treatment process. It was found

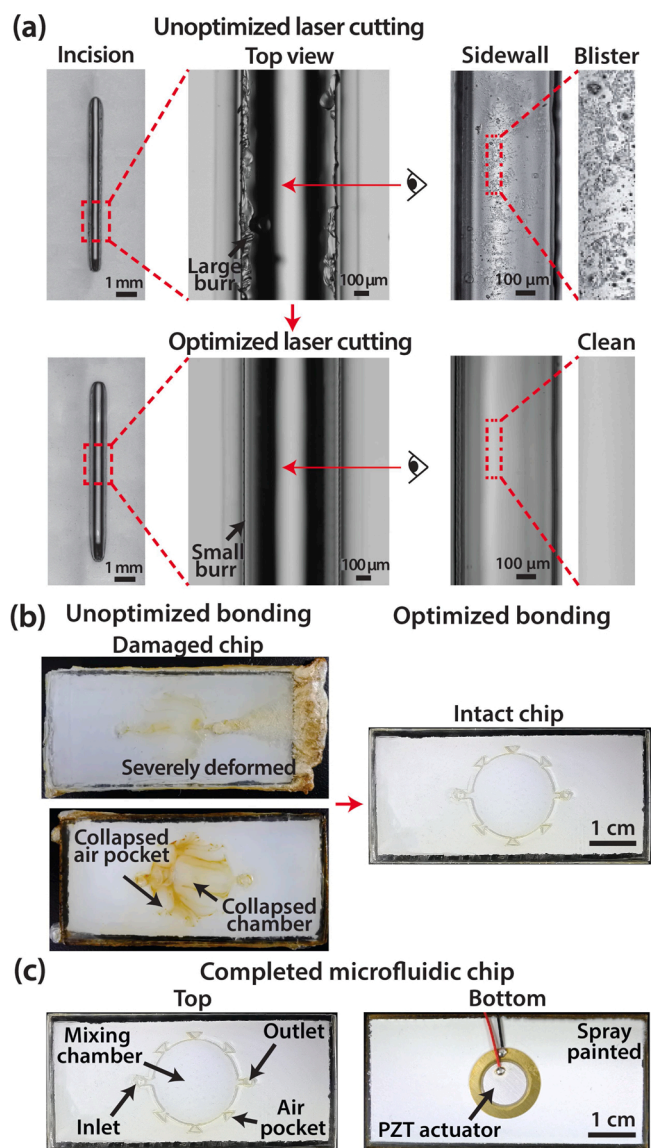


**Fig. 7.** Experimental determination of fabrication conditions. (a) Laser machining of 10-mm incision on 500- $\mu$ m-thick PC sheets was performed by varying cutting parameters; P (power), S (speed), and F (frequency). With an unoptimized condition (P = 3 %, S = 1 %, F = 5000 Hz), a representative section of the incision showed a significant burr in the middle inset figure. The figure on the right, accompanied by an inset figure, shows the rough and blistered inner sidewall. With the optimized condition (P = 6 %, S = 3 %, F = 5000 Hz), the inset figures confirm minimized burr and clean inner sidewall without blisters. (b) Solvent-treatment and thermal-bonding parameters were also experimentally determined. The left panel shows two microfluidic chips fabricated using unoptimized conditions indicating a range of failures (i.e., collapsed microfeatures to fully damaged chip):  $h_{s-s} = 13$  mm,  $t_e = 20$  min,  $T_b = 125$  °C,  $P_b = 1250$  Psi, and  $t_b = 30$  min for the top sample; and the same parameter except  $t_e = 10$  min and  $t_b = 20$  min for the bottom sample. The right panel shows a chip fabricated using the optimized condition ( $h_{s-s} = 13$  mm,  $t_e = 2$  min,  $T_b = 125$  °C,  $P_b = 1250$  psi, and  $t_b = 15$  min) with no leakage and excellent dimensional integrity; 1.85 % of width, 1.56 % of length, and 14.6 % of height reductions from the designed dimension were observed. (c) A microfluidic chip was microfabricated in  $\sim 25$  min using the pre-determined process conditions, followed by gluing a PZT transducer.

that longer  $t_e$  led to more adhesive surfaces but an increased deformation of microfluidic features and translucent surfaces in extreme cases. Conversely, we noted that surface adhesiveness and microfeature deformation reduced when the PC layers were suspended farther from

the surface of the solvent pool (i.e., larger  $h_{s-s}$ ; Fig. 2c) [82]. It was found that the effect of  $t_e$  was more pronounced compared to  $h_{s-s}$ . Thus,  $h_{s-s}$  was fixed to 13 mm, and  $t_e$  was varied to obtain a PC layer with undeformed microfluidic features while maintaining surface adhesiveness. Substantially low  $t_e$  ( $< 1.5$  min) led to a loose bonding that eventually yielded leakage. On the contrary, significantly high  $t_e$  ( $> 5$  min) caused deformation of microfluidic features or collapse of an entire microfluidic chip during later bonding step. Thus, we experimentally determined the optimal  $t_e$  as 2 min, away from both extremes.

Process parameters for thermal bonding are also experimentally determined. Bonding time ( $t_b = 5$ –30 min), bonding temperature ( $T_b = 40$ –125 °C), and bonding pressure ( $P_b = 110$ –1250 Psi) were examined. Extremely high  $P_b$  (1500 Psi) and  $T_b$  (135 °C) caused a significant disfigurement of the microfluidic chip. Moderately high  $P_b$  (1000–1250 Psi) and  $T_b$  (100–125 °C) guaranteed effective bonding when accompanied with intermediate  $t_b$  (10–20 min). However, substantially low  $t_b$  ( $< 10$  min) created weakly bonded PC layers, causing leakage even at high  $P_b$  and  $T_b$ . Thus,  $P_b$  and  $T_b$  were fixed to 1250 Psi and 125 °C respectively while the optimal  $t_b$  was investigated. We observed that effective bonding occurs as  $t_b$  increases but extremely long  $t_b$  causes severe chip deformation or internal damage. Accordingly, 15 min was found to be the optimal  $t_b$  value.

Using unoptimized solvent-treatment and thermal-bonding parameters lead to shrinkage of microfluidic features (i.e., chamber and channels) or even collapse of an entire microfluidic chip. Fig. 7b (left panel) shows outcomes of unoptimized fabrication. The entire chip on the top was severely damaged ( $t_e = 20$  min,  $h_{s-s} = 13$  mm,  $P_b = 1250$  Psi,  $T_b = 125$  °C and  $t_b = 30$  min). The chip on the bottom was internally damaged, exhibiting collapse of air pocket and chamber, and constricted channels ( $t_e = 10$  min,  $h_{s-s} = 13$  mm,  $P_b = 1250$  Psi,  $T_b = 125$  °C and  $t_b = 20$  min). As stated earlier, we noted solvent-exposure time  $t_e$  among other parameters played a significant role in the dimensional integrity of the microfluidic chip. For example, even with optimized  $T_b$ , and lower  $P_b$  and  $t_b$  than the optimal values, excessively large  $t_e$  (i.e.,  $t_e = 30$  min,  $h_{s-s} = 13$  mm,  $P_b = 700$  Psi,  $T_b = 125$  °C, and  $t_b = 5$  min) resulted in significant chip damage, similar to the damaged chip in the left panel of Fig. 7b. Therefore,  $t_e$  was set to 2 min as stated earlier. Fig. 7b (right panel) shows a chip fabricated with an optimized condition where all the microfluidic features and the chip exterior were well preserved. The optimized parameters were  $t_e = 2$  min,  $h_{s-s} = 13$  mm,  $P_b = 1250$  Psi,  $T_b = 125$  °C, and  $t_b = 15$  min.

The completed microfluidic chip is shown in Fig. 7c. It has excellent exterior and interior dimensional accuracy. The measured width and length were 98.1 % and 98.4 % of the designed dimension (28.5 mm and 60 mm), respectively. However, the measured height of the chip was 85.3 % of the designed value (1.5 mm), which was expected from hot pressing. The chamber volume was decreased to 80 % of the designed value (125  $\mu$ L), which is speculated to be the compound effect of a decrease in the length, width, and thickness. Therefore, we deliberately oversized the chamber volume to achieve the required chamber volume (100  $\mu$ L) after bonding. Further optimization of bonding parameters may improve the height-reduction problem in the future. The bottom of the chip was painted white to serve as a high-contrast background for seeded black magnetic beads during assay visualization (Section 2.3.4). The glued PZT actuator is also shown in Fig. 7c (right panel). The overall time taken to fabricate the chip was approximately 25 min, which is notably better than those of previously reported microfluidic cell lysis and DNA extraction devices and/or acoustic-based micromixers based on standard photolithography, soft lithography, hot embossing, and micromilling (i.e., 1–6 h) [32,39,41,56,60]. It should be noted that the painting time was not accounted in counting the fabrication time because coloring will not be necessary for running actual assays.

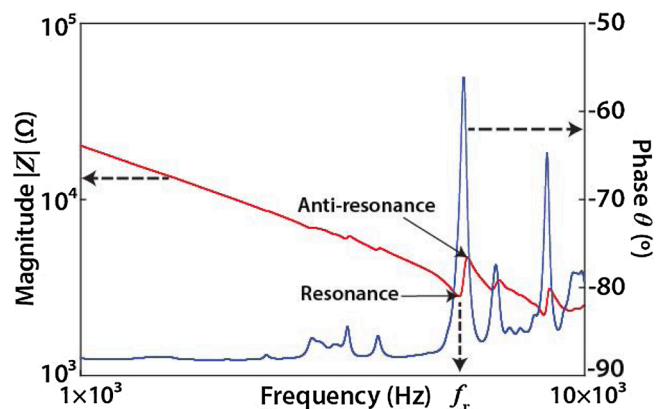


**Fig. 8.** Impedance plot for a microfluidic chip bonded with a PZT transducer. A frequency band of 1–10 kHz was tested for impedance measurement. The strongest resonance signature (i.e., largest magnitude difference between a resonance peak and an anti-resonance peak  $\Delta|Z|$  and the highest positive phase difference  $\Delta\theta$ ) appeared at 5.64 kHz, which was determined as the fundamental flexural resonance frequency. Minor signatures were also observed (e.g., 3.35, 6.54, and 8.31 kHz).

### 3.2. Excitation frequency determination based on electrical impedance measurement

The resonance frequency  $f_r$  of the PZT transducer provided by the manufacturer (Murata) was  $6.0 \pm 1.0$  kHz. Impedance measurement of the PZT transducer exhibited the strongest resonance signature (i.e., the largest magnitude difference  $\Delta|Z|$  between a resonance peak and an anti-resonance peak with the largest phase-angle difference  $\Delta\theta$ ) within the specified frequency range; the  $f_r$  of the PZT transducer was  $5.93 \pm 0.06$  kHz ( $n = 10$ ) (see Section S.7 in SI for more detail).

After confirming that impedance-based  $f_r$  determination was feasible, we measured  $f_r$  of the microfluidic chip. The strongest resonance signature was clearly observed at 5.64 kHz ( $\Delta|Z| = 1860.8 \Omega$  and  $\Delta\theta = 28.1^\circ$ , Fig. 8), which may correspond to the fundamental flexural mode of the microfluidic chip [65]. Additional resonance signatures were also observed at higher and lower frequencies along the impedance spectrum, all exhibited a significantly smaller  $\Delta|Z|$  and  $\Delta\theta$  values (e.g.,  $\Delta|Z| = 912.1$ ,  $\Delta\theta = 18.5$  at 8.31 kHz). We tested several microfluidic chips ( $n = 8$ ), and the fundamental flexural resonance frequency  $f_r$  exhibited a variation of  $5.69 \pm 0.5$  kHz. We speculate that this variation is due to dimensional discrepancy between the chips (e.g., variations in machining errors, alignment errors in thermal bonding and centering errors for the PZT transducer) and due to the difference in vibration dynamics of the transducer.  $f_r$  of a microfluidic chip was individually measured for excitation before cell lysis and DNA extraction assay to account for this  $f_r$  variation.

### 3.3. Experimental determination of air-pocket shape

Once fabrication parameters for laser cutting, solvent exposure, and thermal bonding were determined, we designed the shape of air pockets ( $w$ ,  $h$ , and  $\theta$  of Fig. 1c). Previous work by our research group, where a similar chamber geometry and an air-pocket shape were used for a study of cavitation-microstreaming-based mixing, investigated the impact of the pocket shape on the stability of oscillating bubbles and the effectiveness of microstreaming [65]. The study found that an entrance angle of  $45^\circ$  showed the longest bubble lifetime (i.e., the time before the air pocket was flooded), compared to other angles tested ( $30^\circ$ ,  $60^\circ$ , and  $75^\circ$ ). With a fixed  $45^\circ$  entrance angle ( $\theta$ ), entrance width  $w_e$  that generates the largest mixing zone (i.e., area covered by cavitation microstreaming) was experimentally determined in this study (Fig. 9). The base width  $w$  was fixed to 3 mm but the height  $h$  varied accordingly to maintain  $\theta = 45^\circ$ . A range of entrance width (i.e.,  $w_e = 400, 600, 800,$  and  $1500 \mu\text{m}$ ,

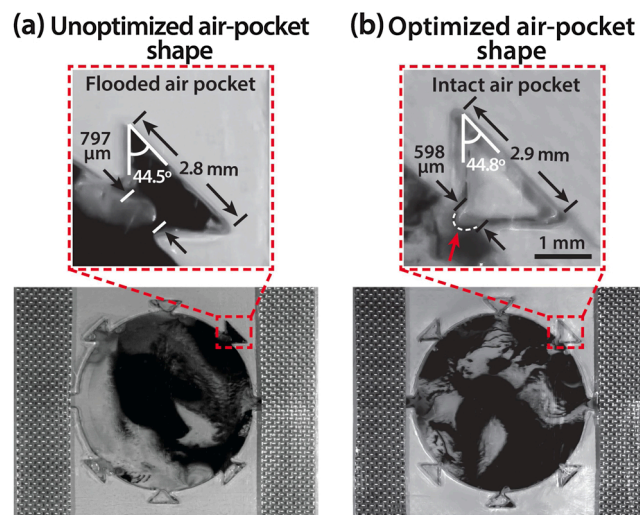


**Fig. 9.** Experimental determination of air-pocket shape. (a) Entrance angle  $\theta$  was maintained at  $45^\circ$  for the longest bubble lifetime, according to our previous study [65]. The entrance width of an inverted-triangular air pocket ( $w_e$ ) was varied for a broad mixing zone and long bubble lifetime ( $>10$  min). An unoptimized air pocket ( $w_e = 797 \mu\text{m}$ ,  $w = 2.8$  mm, note: measured dimension) was flooded quickly ( $\sim 5$  s) after excitation started (inset figure). All air pockets were flooded before  $\sim 5$  min. (b) All of the optimized air pockets ( $w_e = 598 \mu\text{m}$ ,  $w = 2.9$  mm) remained intact during the agitation for up to  $\sim 8$  min (inset figure). Two bubbles remained active for an additional 3–5 min.

note: designed dimension) was tested to obtain the broadest mixing zone and a bubble lifetime larger than the longest mixing time required in the assay steps ( $\sim 10$  min, Section S.1 in SI). Each test chip was excited at its individually measured resonance frequency (Section 3.2).

We observed that the mixing zone became wider and the air pockets were flooded faster (i.e., shorter bubble lifetime) for larger  $w_e$  during excitation (Fig. 9a). On the contrary, bubbles trapped in air pockets of smaller  $w_e$  tended to have a longer lifetime, although the mixing zone was smaller. At  $w_e = 400$  and  $600 \mu\text{m}$ , bubbles were reproducibly formed for all assay steps while some bubbles are instantly flooded at the larger  $w_e$  values. At  $w_e$  of  $600 \mu\text{m}$ , most bubbles survived for up to 8 min of excitation, and two or three bubbles were active more than the targeted 10 min. Also, a mixing zone was broad enough for effective mixing (Fig. 9b). Accordingly, we determined  $w_e$  as  $600 \mu\text{m}$  for the design of our microfluidic chip.

### 3.4. Study of cavitation microstreaming and assay using imaging

We monitored the whole cell lysis and DNA extraction processes using the custom-built imaging setup (Fig. 5). Fig. 10 represents the critical assay steps from lysis-mixture loading to DNA elution (Steps 1–15 of Table S1 in SI). Visual observation helped to establish an assay protocol. Additionally, real-time assay monitoring assisted smooth operation.

A thoroughly cleaned microfluidic chip was prepared (Fig. 10a). Mixture I (i.e., ethanol and magnetic beads) and mixture II (i.e., cell sample, lysis buffer, and Proteinase K) were sequentially loaded to be mixed inside the microchamber (Fig. 10b). This type of sequential loading of separate mixtures is adopted from previous works where off-chip lysis but on-chip DNA extraction was performed; loading the silica magnetic beads and lysed cells separately ensured that DNA extraction strictly occurred inside a microfluidic device for fair performance characterization [32,33]. In our work, both lysis and DNA extraction are conducted inside the chip. Thus, mixture II is prepared off-chip briefly ( $\sim 3$  s) and quickly loaded to the chip ( $\sim 7$  s). By doing so, we ensured that lysis and DNA extraction practically proceeded only on chip for accurate performance characterization. Moreover, by blending the two

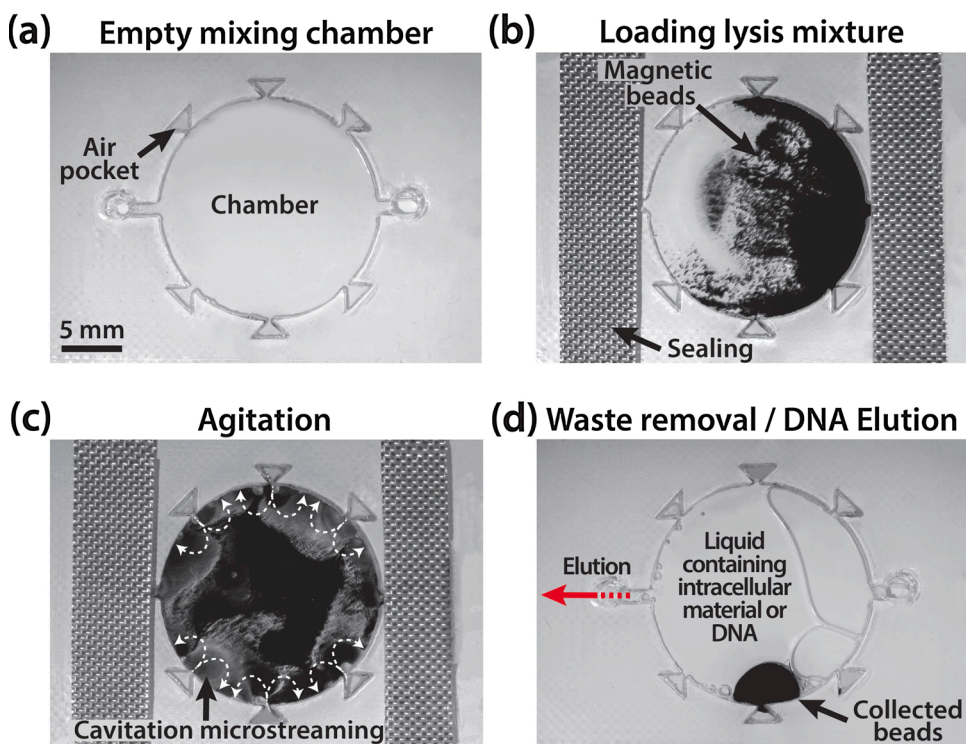


**Fig. 10.** Snapshots of the assay workflow from lysis-mixture loading to DNA elution steps. (a) A microchamber was thoroughly cleaned and ready for loading. (b) Mixture I (ethanol and magnetic beads) and mixture II (cell sample, lysis buffer, and Proteinase K) were loaded consecutively. Beads were not evenly distributed inside the chamber due to the sequential loading of mixture I and II. The inlet and outlet ports were tightly sealed using a Teflon tape to prevent leakage. (c) The chip was excited at its measured flexural resonance frequency  $f_r$  to generate effective agitation inside the microchamber. The white arrows indicate the direction of cavitation microstreaming generated by the oscillating bubbles. The solution was rapidly homogenized, evidenced by a more uniform distribution of beads. Cell lysis and subsequent DNA attachment to the silica surface of the magnetic bead were assisted by agitation. (d) Agitation was halted by turning off the PZT transducer. DNA-bound magnetic beads were collected using a permanent magnet. Then the liquid containing intracellular materials was removed. Steps (b)–(d) were repeated for the subsequent two purification steps and the final DNA elution step.

mixtures of clear color difference (i.e., black mixture I and clear mixture II), the homogenization capability of our device was visually examined. As described in Step 2 of Section 2.7.2, a challenge in sequential loading of the two mixtures due to bubble formation was addressed by our special loading technique. Fig. 10b shows that beads were not evenly distributed due to this sequential loading of mixture I (black) and II (clear). However, the two mixtures were quickly homogenized by cavitation microstreaming in subsequent steps (Fig. 10c). After mixture loading, bubbles were successfully formed in all air pocket for cavitation microstreaming (Fig. 10b). After loading, the inlet and outlet ports were tightly sealed with Teflon tape using an artist's roller. The tape was replaced in subsequent steps to prevent leakage.

Cavitation microstreaming and subsequent agitation ensued as soon as the PZT transducer was turned on (Fig. 10c). Upon excitation of the microfluidic chip at the predetermined  $f_r$ , oscillating bubbles created a strong circulatory flow from the vibrating air-liquid interface. The white arrows approximately indicate the direction of streaming. The DNA-bound magnetic beads were collected into a compact aggregate at the microchamber edge (Fig. 10d) using a unique collection technique we devised (Step 4 in Section 2.7.2). We resorted to this technique because accumulating settled beads, after agitation is off, was substantially slower (possibly due to interaction with the chamber bottom). We collected the beads at the chamber edge because complete aspirating of processed liquid was challenging when the beads were collected at the center; a substantial portion of liquid (~8 %) was trapped around the bead aggregate at the center. This remnant liquid, if carried over to subsequent assay steps, could affect the quality of extracted DNA [41]. Moreover, unlike one at the edge, the aggregate at the center interfered with loading by trapping bubble. After the DNA-bound magnetic beads were collected, unnecessary intracellular materials (i.e., RNA, protein, lipid, etc.) were removed from the microchamber by suction (Fig. 10d). Reagent loading and agitation, bead collection, and aspiration of waste followed a similar process in subsequent steps detailed in Section 2.7.2.

A short assay time is important for high throughput. We somewhat reduced assay time by briefly optimizing mixing time of key assay steps. For example, we tested 2 min, 5 min, and 10 min mixing times for lysis. Since a notable increase in extraction efficiency was not observed after 5

min, we selected 5 min without further attempts. Similarly, a washing time of 1.5 min and 10 min and elution time of 2 min, 10 min, and 20 min were tested. Since reduction of washing time created no significant difference in extraction efficiency and purity, we selected 1.5 min. On the contrary, higher extraction efficiency was observed for increasing elution time, although it was largely the same after 10 min. Thus, an elution time of 10 min was selected.

The total assay time from the mixture-I loading to DNA elution including manual handling (e.g., securing and detaching of the jig from XY stage, liquid loading and removal) was 25.4 min. Our assay throughput would be twice higher than that of the commercial kit (Magazorb DNA Mini-Prep Kit) as it took 54.5 min (60 min specified by the manufacturer [87]) for us to complete the same task using microcentrifuge tubes. Other magnetic-bead-based commercial kits, including MagAttract HMW DNA Kit (Qiagen) [88] and BioVision cell & tissue genomic DNA extraction kit (BioVision) [89], require 40~70 min of assay time with the exception of few kits, for example, 20 min of ID Gene MagFast Universal Purification Kit (Labgene Scientific) [90] designed to be used in an automated system. Silica-column-based kits also typically have faster assay time, for example, 20 min of Wizard SV Genomic DNA Purification System (Promega) [87]. However, these kits rely on a centrifuge, which is impractical for a microfluidic device.

We also attempted to compare our assay time with those of similar microfluidic assays [32,33,37,39,41,56]. Including manual handling time, our assay time was comparable with those of microfluidic chemical lysis and DNA-extraction works (e.g., 20 min [39]). Excluding the manual handling time, ours, including both *on-chip* lysis and DNA extraction, was comparable to those of previous *on-chip* DNA extraction yet *off-chip* lysis works (e.g., ~20 min [37,41], ~22 min [32,33]) and was much faster than that of *on-chip* cell-free DNA extraction work (42 min [56]). Therefore, our proof-of-concept assay could be faster if compared head-to-head with these previous works. We believe the assay time can be reduced further by reducing mixing time of each assay step which collectively takes 71 % of the total assay time. Additionally, incorporating vertically hanging air pockets could facilitate out-of-plane mixing in the Z-direction (i.e., in addition to the existing 2D planar mixing), which could lead to improved assay time (see Section 3.5.2).

**Table 1**

Summary of DNA-extraction results using the microfluidic chip and commercial kit.

Method	Cell line	Average concentration (ng/ $\mu$ L)	Average purity (A <sub>260</sub> /A <sub>280</sub> )	Chip-to-kit concentration ratio
Microfluidic chip	K562	16.8 $\pm$ 3.23 <sup>a</sup>	1.87 $\pm$ 0.10	0.849
Commercial kit		19.8 $\pm$ 2.66	2.01 $\pm$ 0.08	
Microfluidic chip	CHO-K1	9.48 $\pm$ 1.31 <sup>a</sup>	1.85 $\pm$ 0.13	0.837
Commercial kit		11.3 $\pm$ 1.80	2.09 $\pm$ 0.13	

<sup>a</sup> The concentration measured by the spectrophotometer was adjusted 0.5 $\times$  as the elution volume from the microfluidic chip was also 0.5 $\times$  of that from the commercial kit.

### 3.5. Assay performance analysis

#### 3.5.1. Determination of concentration and purity

The performance of our microfluidic chip, and the associated cell-lysis and DNA-extraction assay were evaluated using two different mammalian cell lines, K562 and CHO-K1. First, we tested the K562 cell (i.e., myelogenous leukemia cell line) as it is widely used in biomedical research [91]. Moreover, these round and non-adherent cells have reduced clumping compared to other cell suspensions, advantageous for our assay development [92]. Experimental results exhibit that the performance of our microfluidic chip is comparable to that of the commercial kit (Table 1). The concentration of DNA extracted using the microfluidic chip was 16.8  $\pm$  3.23 ng/ $\mu$ L ( $n = 5$ , cell number = 1.73  $\times 10^5$ ). For the same number of cells, a DNA concentration of 19.8  $\pm$  2.66 ng/ $\mu$ L ( $n = 5$ ) was obtained using the commercial kit (MagaZorb DNA Mini-Prep kit). The DNA concentration from our microfluidic chip was less (15.1 %) than that of the commercial kit. The purity (A<sub>260</sub>/A<sub>280</sub>) of the extracted DNA was 1.87  $\pm$  0.1 for the microfluidic chip and 2.01  $\pm$  0.08 for the kit (Table 1). Both values satisfied the purity requirement 1.7–2.0 for downstream applications.

DNA was also extracted from the CHO-K1 cells, another frequently used mammalian epithelial cell [93], to further evaluate our assay with a non-human cell line and, more importantly, to quantify extraction efficiency later (Section 3.5.2). Using CHO-K1 cells, the concentration of DNA extracted using the microfluidic chip and kit was 9.48  $\pm$  1.31 ng/ $\mu$ L ( $n = 5$ ) and 11.3  $\pm$  1.80 ng/ $\mu$ L ( $n = 5$ ) respectively with a purity of 1.85  $\pm$  0.13 and 2.09  $\pm$  0.13 respectively from 4.56  $\times 10^5$  cells. The concentration of DNA from our microfluidic chip was also less (16.1 %) than that of the commercial kit. In order to confirm whether cavitation microstreaming significantly enhanced the chemical cell lysis and magnetic-bead-based DNA extraction, a control experiment was conducted. The same protocol was performed in a similarly-shaped microchamber without air pockets, thus generating no cavitation microstreaming (note: the chip was still agitated). For the same number of CHO-K1 cells, the DNA concentration was substantially low: only 58.9 % of the normal case (5.59  $\pm$  1.15 ng/ $\mu$ L,  $n = 5$ ). Its purity was also out of range (2.98  $\pm$  0.79).

The amount of DNA extracted using our microfluidic chip was on average 85 % of the amount extracted using the commercial kit, which is a well-established method. The excellent purity also proves its applicability for downstream analysis. The attained result is remarkable considering that our proof-of-concept microfluidic chip and assay were not rigorously optimized (see Section 3.5.2 for detail).

#### 3.5.2. Determination of extraction efficiency

Extraction efficiency (i.e., the ratio of the recovered DNA mass to the loaded DNA mass) is an important figure of merit because it gauges the capability of DNA extraction with minimal material loss [37] and can be

**Table 2**

Comparison of extraction efficiency for the microfluidic chip and the commercial kit using CHO-K1 cell.

Description	Chip	Kit
Number of cells/sample	4.56 $\times 10^5$	
Genomic DNA mass (pg/cell)	5.4	
Measured concentration (ng/ $\mu$ L)	9.48 <sup>a</sup>	11.3
Elution volume ( $\mu$ L)	200	
Theoretical DNA yield (ng)	2464	
Measured DNA yield (ng)	1896	2264
Extraction efficiency (%)	76.9	91.9

<sup>a</sup> The concentration measured by the spectrophotometer was adjusted 0.5 $\times$  as the elution volume from the microfluidic chip was also 0.5 $\times$  of that from commercial kit.

used to compare with other methods regardless of sample volume or concentration. The K562 cell has inherently varying DNA mass due to polyploidy, a condition where some cells contain more than two paired sets of chromosomes [94]. Therefore, it was challenging to calculate extraction efficiency using K562 cell as a unique DNA mass (e.g., 6.25 pg DNA/cell for human white blood cell) could not be assumed. Instead, the CHO-K1 cell with a known DNA mass (5.4 pg/cell) [95] was used to estimate extraction efficiency. The extraction efficiency of the microfluidic chip was calculated to be 76.9 % using the DNA mass (pg/cell), cell number, and concentration of the extracted DNA (ng/ $\mu$ L) (Table 2). The extraction efficiency of the commercial kit was also characterized in the same manner (91.9 %). The extraction efficiency of the microfluidic chip was 16.2 % less than that of the commercial kit.

Although appeared outstanding for a proof-of-concept device, the extraction efficiency of our microfluidic device is lower than that of the commercial kit. We speculated that the reasons are twofold: under-optimized assay protocol and chip design. The protocol for the commercial kit has been well optimized and proven by users. Our protocol, on the other hand, was briefly developed (Section 3.4) to prove the novel concept of cavitation-microstreaming-based cell lysis and DNA extraction, which is the scope of this work.

For a chip design aspect, we speculated that the liquid volume relative to the active (agitation-inducing) area is an important parameter affecting mixing performance [65].  $R_{sv}$ , the ratio of active surface (e.g., moving air-water interface in this work) to mixing volume, was analyzed to evaluate the mixing performance and subsequently the extraction efficiency. Previous researches with similar design and working principle exhibited faster mixing time by having large  $R_{sv}$  values:  $\sim 9$  s for an  $R_{sv}$  of 333 (17 air pockets of 500  $\mu$ m diameter for 10- $\mu$ L mixing volume) [56] and  $\sim 6$  s for an  $R_{sv}$  of 137 (35 air pockets of 500  $\mu$ m diameter for 50- $\mu$ L mixing volume) [58]). In contrast,  $R_{sv}$  of our microfluidic chip is only 17. We believe the mixing performance could have improved if we had increased the number of air pockets or decreased the mixing volume.

The better extraction efficiency of the commercial kit may be associated with enhanced mixing in the microcentrifuge tube, which could be related to higher fluid velocity and its 3D structure. For a standard 1.5 mL microcentrifuge tube agitated with a standard laboratory vortex mixer having a maximum rotational speed of 3200 rpm, liquid velocity could reach >1000 mm/s [96]. In contrast, it has been reported that the streaming velocity generated by an oscillating bubble (250- $\mu$ m radius, excited at 5.8 kHz) reaches relatively slower 0.4 mm/s, which may yield less effective mass transport [97]. Moreover, a fluid dynamics study of microscale mixing indicated that a larger mixing chamber height leads to better mixing due to enhanced swirling flow (i.e., out-of-plane flow) [98]. This could explain better mixing inside the microcentrifuge tube, which has a 3D conical shape. In contrast, essentially planar microstreaming from horizontally positioned bubbles in the 2D microchamber (Fig. 1) could limit convective mass transport. We believe the mixing and consequently assay performance could be improved if vertically hanging air pockets are used to facilitate out-of-plane mixing in the

Z-direction in addition to planar mixing [59].

Even with these limitations, our proof-of-concept microfluidic chip has shown notable performance compared to previous microdevices for chemical lysis and DNA extraction. Off-chip lysis followed by dSPE from whole blood sample inside a straight-channel microdevice reported an extraction efficiency of only 64 % [32]. Although extraction from a minuscule sample ( $\sim 0.6 \mu\text{L}$ ) can be a good feat, it required a time-consuming in-cleanroom fabrication process (i.e., glass microfluidic device). A previous study had reported a similar extraction efficiency of 80 % from *E. coli* cells spiked into human blood [41]. However, the complex fabrication, including die cutting, mold making for hot embossing, micromilling, and epoxy-assisted thermal bonding, puts it at a disadvantage. In contrast, our device is much simpler to fabricate and operate but showed a similar or better extraction efficiency for shorter assay time.

### 3.5.3. PCR and gel electrophoresis result

The performance of our microfluidic chip was further evaluated based on qualitative analysis of the extracted DNA using off-chip PCR and gel electrophoresis [23]. Gel electrophoresis images of the PCR-amplified target DNA (pentaplicates, lane 1–5) are shown in Fig. 11. A clear single band at 116 bp in each lane proved that the quality of DNA was excellent and appropriate for downstream analysis (Fig. 11a). A control experiment using the commercial kit (Fig. 11b) demonstrated a similar result, further validating our assay.

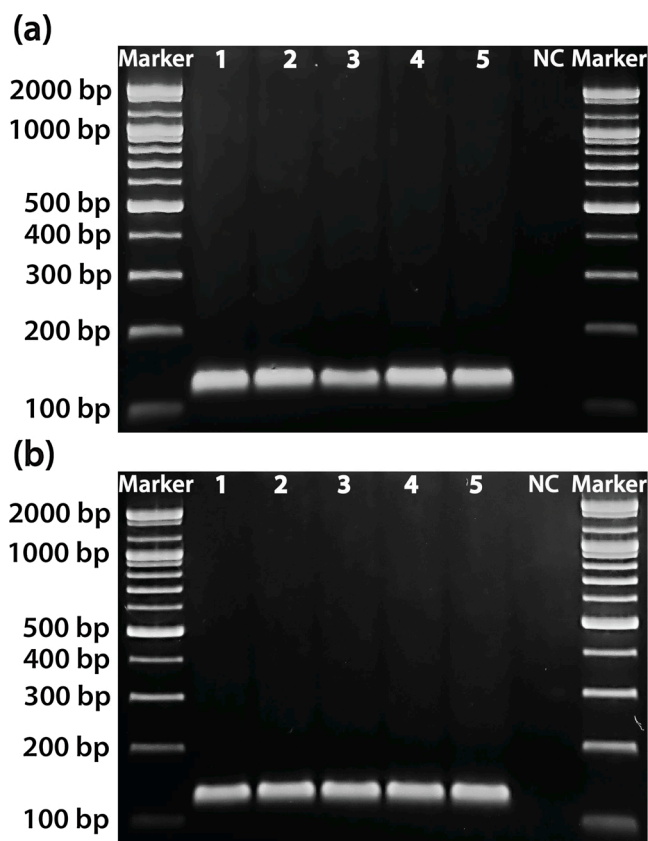


**Fig. 11.** Gel electrophoresis results for an amplified DNA fragment from K562 cells. PCR amplification was conducted using DNA extracted by (a) the microfluidic chip and (b) the Magazorb DNA mini-prep kit (control). The first and last lanes show a 100-bp standard DNA ladder. Lane 1–5 show an amplified vWF gene (116 bp) from DNA extracted and purified from  $1.7 \times 10^5$  K562 cells. NC lane represents negative control and shows no false positives from amplification.

### 3.5.4. Determination of dynamic range and lower limit of extraction

The lower limit of extraction (LOE) of our microfluidic device was also characterized. The LOE is critical when extracting DNA from a rare population of cells. Scarce DNA could adsorb to the various inner surface of the microfluidic chip or during lysis, purification, and elution steps [99]. For K562 cells, samples containing cell numbers ranging from  $1.8 \times 10^1$  to  $1.8 \times 10^5$  were prepared in 100- $\mu\text{L}$  aliquots by a serial dilution from a sample with  $1.8 \times 10^5$  cells. DNA extracted from each cell sample was collected in a 100- $\mu\text{L}$  eluent. Initially, only 3 % volume (3  $\mu\text{L}$ ) of the eluents containing extracted DNA was used for PCR according to a protocol developed by our collaborator (Biomedux). However, due to the small volume of DNA-sample used for amplification, we were not able to detect PCR products from  $1.8 \times 10^1$  to  $1.8 \times 10^3$  cells. The problem was aggravated by a worse limit of detection ( $\sim 140 \text{ pg}$ ) [100] of the staining dye (Dyne loading star).

To address this problem, we first concentrated the DNA sample using a spin column and then improved the PCR protocol. First, we attempted to concentrate extracted DNA using a spin column (ZYMO Research) following the manufacturer's protocol. However, the concentration factor characterized by UV/Vis spectrophotometry was only  $\sim 3$ . Thus, we modified the manufacturer's protocol (i.e., increased centrifugation time of 1 min, binding buffer-DNA incubation time of 10 min, and elution buffer-DNA incubation time of 30 min) and were able to reach a higher concentration factor ( $\sim 6$ ). Secondly, the collaborator-provided PCR protocol was also improved. Initially, 35 amplification cycles were used. After increasing the cycle to 40, the amplification results improved while not generating any false positives. Lastly, DNA sample volume was also increased from 3  $\mu\text{L}$  to 6  $\mu\text{L}$  to improve the PCR result.

DNA extracted from all cell numbers ranging from  $1.8 \times 10^1$  to  $1.8 \times 10^5$  were successfully concentrated  $\sim 6\times$  using the spin column and then amplified using our improved PCR protocol. Fig. 12 indicates the amplified vWF gene from K562 cells from the tested cell number range. The LOE was indicated by unequivocal detection of the target gene from as few as 18 cells (white arrow). Previous works have reported microfluidic chemical lysis and DNA extraction from a large number of cells (i.e.,  $1.5 \times 10^8$  cells [101,102]) as well as a small number of cells (i.e.,  $4.5 \times 10^3$  cells) [32,102]. But these studies did not show “dynamic range” of extraction. In contrast, our device has shown an impressive dynamic range (five orders of magnitude) of processable cell numbers. Another study has reported the extraction of DNA from as small as 10 Jurkat cells using 10  $\mu\text{L}$  elution volume [42], but its elution volume is 10 $\times$  smaller than ours. If the elution volume of our device is the same as theirs, we could detect DNA from even smaller than 18 cells because eluents would be more concentrated. Considering the large elution volume and the fact that DNA can still be extracted from as few as 18 cells, our device has exhibited outstanding performance.

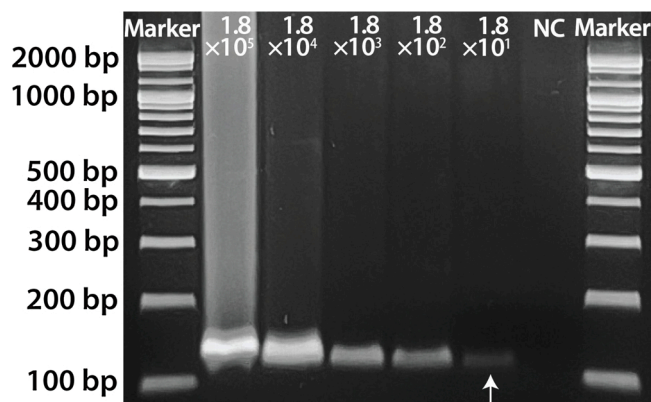


**Fig. 12.** Gel electrophoresis result for amplified DNA fragment from K562 cells. The 2nd to 6th lanes ( $1.8 \times 10^1$ – $1.8 \times 10^5$  cells) show the amplified vWF gene from DNA extracted and purified using the microfluidic chip. The first and last lanes show a 100-bp standard DNA ladder. NC lane represents negative control.

Integration of on-chip DNA amplification is vital in adapting our device for POC NAT applications. Reduction of elution volume (i.e., volume of extracted DNA) to 2~10  $\mu\text{L}$  for PCR amplification [41,103,104] is key for such integration. We are currently working toward a new device design of a reduced chamber volume to meet this requirement since cavitation-microstreaming-based mixing has been demonstrated in a miniscule volume as low as  $\sim 0.4 \mu\text{L}$  [50].

#### 4. Conclusion

The extraction of nucleic acid from a small amount of sample with quality and quantity suitable for subsequent genetic analysis is essential for POC NAT (point-of-care nucleic acid testing) that caught unprecedented attention recently due to the COVID-19 pandemic. Mixing has assisted various steps in the process of cell lysis leading up to DNA extraction by improved mass transport. We proposed to employ cavitation microstreaming due to effective mass transport enabled by exceptionally rapid mixing [50]. The bubbles trapped in air pockets were oscillated, generating strong circulatory bulk flows when the chip was excited at its flexural resonance frequency, determined by an impedance analyzer. This strong streaming facilitated chemical cell lysis and DNA extraction, substantiated by the control experiment using the CHO-K1 cell without cavitation microstreaming. We adopted the magnetic bead-based DNA extraction and purification for its proven performance, compatibility with the streaming-based agitation, and capability for assay visualization.

The laser micromachining condition for polycarbonate (PC) was experimentally determined for minimized burr and reduced cut-sidewall roughness. Solvent treatment of PC layers and subsequent thermal bonding were also fine-tuned to obtain a non-leaking multilayer microfluidic device with a clean inner surface and excellent dimensional integrity. Our cleanroom-free microfabrication process was rapid ( $\sim 25$  min from a CAD design to a completed chip). An affordable PZT transducer ( $\sim \$0.80$ ) was bonded to the bottom of the chip and successfully excited the bubble for cavitation microstreaming.

Our microfluidic device was evaluated by extracting DNA from K562 and CHO-K1 cells. The microfluidic chip showed notable performance without a thorough assay optimization. The concentration of DNA extracted with the chip was also comparable with that of a commercial kit. The extracted DNA has also shown excellent purity, indicating suitability for downstream analysis. Our microfluidic chip has shown an extraction efficiency of 76.9%, which is deemed remarkable considering the planar microchip design and the small oscillating surface-to-chamber volume ratio ( $R_{sv}$ ), and the briefly optimized extraction protocol. We believe that the extraction efficiency could be enhanced further by rigorous optimization of the extraction protocol and improvement in the chip design. It was also noteworthy that our assay from loading sample to DNA elution took only 25.4 min, almost twice faster than that of the commercial magnetic-bead based DNA-extraction kit (i.e., MagaZorb DNA Mini-Prep Kit) used for our control experiment, implying higher assay throughput when linked to downstream analysis. PCR and gel electrophoresis results validated the quality of the extracted and purified DNA and its applicability for downstream processes. The lower limit of extraction (LOE) experiment indicates that cell lysis and DNA extraction were successfully executed from as few as 18 mammalian cells, which is comparable to a previous result which extracted DNA from 10 cells but with notably smaller elution volume (i.e., 10% of our elution volume). The dynamic range of our method was also outstanding, spanning five orders of magnitude.

The simple design, rapid and cleanroom-free fabrication, and micromixing generated by a cost-effective PZT transducer render our device promising for POC NAT applications. We are currently working towards improving the extraction efficiency and assay time by adopting a new design and further optimization of the protocol (e.g., investigating varying reagent compositions and optimizing mixing time of each assay step). In the long run, on-chip nucleic-acid amplification and detection

will be incorporated for a range of clinical targets such as MRSA (methicillin-resistant staphylococcus aureus) and O157:H7 *E.coli*.

#### CRedit authorship contribution statement

**Abdi Mirgissa Kaba:** Writing - original draft, Investigation, Visualization, Data curation, Formal analysis, Validation, Methodology. **Hyunjin Jeon:** Investigation, Visualization, Methodology. **Areum Park:** Investigation, Visualization, Methodology. **Kyungjin Yi:** Investigation. **Seonhyeok Baek:** Investigation. **Aeja Park:** Project administration, Funding acquisition, Resources, Supervision. **Dohyun Kim:** Writing - review & editing, Conceptualization, Methodology, Supervision, Project administration, Funding acquisition, Validation.

#### Declaration of Competing Interest

The authors report no declarations of interest.

#### Acknowledgements

This work (Grant No. S2601365) was supported by project for Cooperative R&D between Industry, Academy, and Research Institute funded by the Korea Ministry of SMEs and Startups in 2018. This work was also supported by Basic Science Research Programs through the National Research Foundation of Korea (NRF) funded by the Korean government (MSIT) (2019R1F1A1043885).

#### Appendix A. Supplementary data

Supplementary material related to this article can be found, in the online version, at doi:<https://doi.org/10.1016/j.snb.2021.130511>.

#### References

- [1] E. Colzani, Beyond morbidity and mortality: the burden of infectious diseases on healthcare services, *Epidemiol. Infect.* 147 (2019) e251.
- [2] T. Vos, S.S. Lim, C. Abbafati, K.M. Abbas, M. Abbasi, M. Abbasifard, M. Abbasi-Kangevari, H. Abbastabar, F. Abd-Allah, A. Abdelalim, et al., Global burden of 369 diseases and injuries in 204 countries and territories, 1990–2019: a systematic analysis for the global burden of disease study 2019, *Lancet* 396 (2020) 1204–1222.
- [3] M.S. Mehand, F. Al-Shorbaji, P. Millett, B. Murgue, The WHO R&D blueprint: 2018 review of emerging infectious diseases requiring urgent research and development efforts, *Antiviral Res.* 159 (2018) 63–67.
- [4] I. Chakraborty, P. Maity, Covid-19 outbreak: migration, effects on society, global environment and prevention, *Sci. Total Environ.* 728 (2020), e138882.
- [5] D.J. Speers, Clinical applications of molecular biology for infectious diseases, *Clin. Biochem. Rev.* 27 (2006) 39–51.
- [6] A. Niemz, T.M. Ferguson, D.S. Boyle, Point-of-care nucleic acid testing for infectious diseases, *Trends Biotechnol.* 29 (2011) 240–250.
- [7] E. Primiceri, M.S. Chiriaco, F.M. Notarangelo, A. Crocamo, D. Ardissino, M. Cereda, A.P. Bramanti, M.A. Bianchessi, G. Giannelli, G. Maruccio, Key enabling technologies for point-of-care diagnostics, *Sensors* 18 (2018) e3607.
- [8] R. Paul, E. Ostermann, Q. Wei, Advances in point-of-care nucleic acid extraction technologies for rapid diagnosis of human and plant diseases, *Biosens. Bioelectron.* 169 (2020), e112592.
- [9] K. Mahesh, S. Vaidya, Microfluidics: a boon for biological research, *Curr. Sci.* 112 (2017) 2021–2028.
- [10] G.M. Whitesides, The origins and the future of microfluidics, *Nature* 442 (2006) 368–373.
- [11] S. Wang, M.A. Lifson, F. Inci, L.-G. Liang, Y.-F. Sheng, U. Demirci, Advances in addressing technical challenges of point-of-care diagnostics in resource-limited settings, *Expert Rev. Mol. Diagn.* 16 (2016) 449–459.
- [12] F. Cui, M. Rhee, A. Singh, A. Tripathi, Microfluidic sample preparation for medical diagnostics, *Annu. Rev. Biomed. Eng.* 17 (2015) 267–286.
- [13] A. Ayoib, U. Hashim, S.C.B. Gopinath, M.K. Md Arshad, DNA extraction on bio-chip: history and preeminence over conventional and solid-phase extraction methods, *Appl. Microbiol. Biotechnol.* 101 (2017) 8077–8088.
- [14] M. Shehadul Islam, A. Aryasomayajula, P.R. Selvaganapathy, A review on macroscale and microscale cell lysis methods, *Micromachines* 8 (2017) e0083.
- [15] J. Kim, M. Johnson, P. Hill, B.K. Gale, Microfluidic sample preparation: cell lysis and nucleic acid purification, *Integr. Biol.* 1 (2009) 574–586.
- [16] A. Berasaluze, L. Matthys, J. Mujika, M. Antonana-Diez, A. Valero, M. Agirregabiria, Bead beating-based continuous flow cell lysis in a microfluidic device, *RSC Adv.* 5 (2015) 22350–22355.

- [17] P.E. Vandeventer, K.M. Weigel, J. Salazar, B. Erwin, B. Irvine, R. Doebler, A. Nadim, G.A. Cangelosi, A. Niemi, Mechanical disruption of lysis-resistant bacterial cells by use of a miniature, low-power, disposable device, *J. Clin. Microbiol.* 49 (2011) e2533.
- [18] D.D. Carlo, K.-H. Jeong, L.P. Lee, Reagentless mechanical cell lysis by nanoscale barbs in microchannels for sample preparation, *Lab Chip* 3 (2003) 287–291.
- [19] C.W. Fung, S.N. Chan, A.R. Wu, Microfluidic single-cell analysis—toward integration and total on-chip analysis, *Biomicrofluidics* 14 (2020), e021502.
- [20] S.-H. Huang, L.-Y. Hung, G.-B. Lee, Continuous nucleus extraction by optically-induced cell lysis on a batch-type microfluidic platform, *Lab Chip* 16 (2016) 1447–1456.
- [21] R.B. Brown, J. Audet, Current techniques for single-cell lysis, *J. R. Soc. Interface* 5 (2008) 131–138.
- [22] P.A. Quinto-Su, H.-H. Lai, H.H. Yoon, C.E. Sims, N.L. Allbritton, V. Venugopalan, Examination of laser microbeam cell lysis in a pdms microfluidic channel using time-resolved imaging, *Lab Chip* 8 (2008) 408–414.
- [23] K. Tsougeni, A.S. Kastania, G.D. Kaprou, M. Eck, G. Jobst, P.S. Petrou, S. E. Kakabakos, D. Mastellos, E. Gogolides, A. Tserepi, A modular integrated lab-on-a-chip platform for fast and highly efficient sample preparation for foodborne pathogen screening, *Sens. Actuators B Chem.* 288 (2019) 171–179.
- [24] J.C. Weaver, Electroporation of cells and tissues, *IEEE Trans. Plasma Sci.* 28 (2000) 24–33.
- [25] X.-y. Wei, J.-h. Li, L. Wang, F. Yang, Low-voltage electrical cell lysis using a microfluidic device, *Biomed. Microdevices* 21 (2019) e022.
- [26] C. Church, J. Zhu, G. Huang, T.-R. Tzeng, X. Xuan, Integrated electrical concentration and lysis of cells in a microfluidic chip, *Biomicrofluidics* 4 (2010) 44101.
- [27] D.W. Lee, Y.-H. Cho, A continuous electrical cell lysis device using a low dc voltage for a cell transport and rupture, *Sens. Actuators B Chem.* 124 (2007) 84–89.
- [28] M.B. Fox, D.C. Esveld, A. Valero, R. Luttg, H.C. Mastwijk, P.V. Bartels, A. van den Berg, R.M. Boom, Electroporation of cells in microfluidic devices: a review, *Anal. Bioanal. Chem.* 385 (2006) e474.
- [29] L. Nan, Z. Jiang, X. Wei, Emerging microfluidic devices for cell lysis: a review, *Lab Chip* 14 (2014) 1060–1073.
- [30] J. Leipter, A. Tholey, Miniaturized sample preparation on a digital microfluidics device for sensitive bottom-up microproteomics of mammalian cells using magnetic beads and mass spectrometry-compatible surfactants, *Lab Chip* 19 (2019) 3490–3498.
- [31] W. Qamar, M.R. Khan, A. Arafah, Optimization of conditions to extract high quality DNA for PCR analysis from whole blood using sds-proteinase k method, *Saudi J. Biol. Sci.* 24 (2017) 1465–1469.
- [32] G.R.M. Duarte, C.W. Price, J.L. Littlewood, D.M. Haverstick, J.P. Ferrance, E. Carrilho, J.P. Landers, Characterization of dynamic solid phase DNA extraction from blood with magnetically controlled silica beads, *Analyst* 135 (2010) 531–537.
- [33] G.R.M. Duarte, C.W. Price, B.H. Augustine, E. Carrilho, J.P. Landers, Dynamic solid phase DNA extraction and PCR amplification in polyester-toner based microchip, *Anal. Chem.* 83 (2011) 5182–5189.
- [34] A. Bhattacharyya, C.M. Klapperich, On-chip cell lysis, in: D. Li (Ed.), *Encyclopedia of Microfluidics and Nanofluidics*, Springer New York, New York, NY, 2015, pp. 2481–2483.
- [35] S.C. Tan, B.C. Yip, DNA, RNA, and protein extraction: The past and the present, *J. Biomed. Biotechnol.* 2009 (2009), e574398.
- [36] A. Dhaliwal, DNA extraction and purification, *Mater. Methods* 3 (2013).
- [37] K.R. Jackson, J.C. Borba, M. Meija, D.L. Mills, D.M. Haverstick, K.E. Olson, R. Aranda, G.T. Garner, E. Carrilho, J.P. Landers, DNA purification using dynamic solid-phase extraction on a rotationally-driven polyethylene-terephthalate microdevice, *Anal. Chim. Acta* 937 (2016) 1–10.
- [38] M.C. Breamore, K.A. Wolfe, I.G. Arcibal, W.K. Leung, D. Dickson, B.C. Giordano, M.E. Power, J.P. Ferrance, S.H. Feldman, P.M. Norris, et al., Microchip-based purification of DNA from biological samples, *Anal. Chem.* 75 (2003) 1880–1886.
- [39] X. Chen, D.F. Cui, C.C. Liu, On-line cell lysis and DNA extraction on a microfluidic biochip fabricated by microelectromechanical system technology, *Electrophoresis* 29 (2008) 1844–1851.
- [40] C.W. Price, D.C. Leslie, J.P. Landers, Nucleic acid extraction techniques and application to the microchip, *Lab Chip* 9 (2009) 2484–2494.
- [41] S.M. Azimi, G. Nixon, J. Ahern, W. Balachandran, A magnetic bead-based DNA extraction and purification microfluidic device, *Microfluid. Nanofluid.* 11 (2011) 157–165.
- [42] U. Lehmann, C. Vandevyver, V.K. Parashar, M.A.M. Gijs, Droplet-based DNA purification in a magnetic lab-on-a-chip, *Angew. Chem. Int. Ed.* 45 (2006) 3062–3067.
- [43] G.S. Jeong, S. Chung, C.B. Kim, S.H. Lee, Applications of micromixing technology, *Analyst* 135 (2010) 460–473.
- [44] K. Ward, Z.H. Fan, Mixing in microfluidic devices and enhancement methods, *J. Micromech. Microeng.* 25 (2015), e094001.
- [45] C.-Y. Lee, L.-M. Fu, Recent advances and applications of micromixers, *Sens. Actuators B Chem.* 259 (2018) 677–702.
- [46] C.-Y. Lee, W.-T. Wang, C.-C. Liu, L.-M. Fu, Passive mixers in microfluidic systems: a review, *Chem. Eng. J.* 288 (2016) 146–160.
- [47] Y. Suh, K. Sangmo, A review on mixing in microfluidics, *Micromachines* 1 (2010) 82–111.
- [48] L.A.N. Julius, V.K. Jagannadh, I.J. Michael, R. Srinivasan, S.S. Gorthi, Design and validation of on-chip planar mixer based on advection and viscoelastic effects, *Biochip J.* 10 (2016) 16–24.
- [49] N.Y. Lee, M. Yamada, M. Seki, Development of a passive micromixer based on repeated fluid twisting and flattening, and its application to DNA purification, *Anal. Bioanal. Chem.* 383 (2005) 776–782.
- [50] D. Ahmed, X. Mao, J. Shi, B.K. Juluri, T.J. Huang, A millisecond micromixer using single-bubble-based acoustic streaming, *Lab Chip* 9 (2009) 2738–2741.
- [51] X. Niu, Y.-K. Lee, Efficient spatial-temporal chaotic mixing in microchannels, *J. Micromech. Microeng.* 13 (2003) 454–462.
- [52] Y. Wang, J. Zhe, B.T.F. Chung, P. Dutta, A rapid magnetic particle driven micromixer, *Microfluid. Nanofluid.* 4 (2008) 375–389.
- [53] B. Xu, T.N. Wong, N.-T. Nguyen, Z. Che, J.C.K. Chai, Thermal mixing of two miscible fluids in a T-shaped microchannel, *Biomicrofluidics* 4 (2010), e044102.
- [54] E. Choi, B. Kim, J. Park, High-throughput microparticle separation using gradient traveling wave dielectrophoresis, *J. Micromech. Microeng.* 19 (2009), e125014.
- [55] A. Ozelcik, D. Ahmed, Y. Xie, N. Nama, Z. Qu, A.A. Nawaz, T.J. Huang, An acoustofluidic micromixer via bubble inception and cavitation from microchannel sidewalls, *Anal. Chem.* 86 (2014) 5083–5088.
- [56] A.J. Conde, I. Keraite, A.E. Ongaro, M. Kersaudy-Kerhoas, Versatile hybrid acoustic micromixer with demonstration of circulating cell-free DNA extraction from sub-ml plasma samples, *Lab Chip* 20 (2020) 741–748.
- [57] M. Wiklund, R. Green, M. Ohlin, Acoustofluidics 14: applications of acoustic streaming in microfluidic devices, *Lab Chip* 12 (2012) 2438–2451.
- [58] R.H. Liu, R. Lenigk, R.L. Druyor-Sanchez, J. Yang, P. Grodzinski, Hybridization enhancement using cavitation microstreaming, *Anal. Chem.* 75 (2003) 1911–1917.
- [59] R.H. Liu, J. Yang, M.Z. Pindera, M. Athavale, P. Grodzinski, Bubble-induced acoustic micromixing, *Lab Chip* 2 (2002) 151–157.
- [60] M.R. Rasouli, M. Tabrizian, An ultra-rapid acoustic micromixer for synthesis of organic nanoparticles, *Lab Chip* 19 (2019) 3316–3325.
- [61] J.A. Rooney, Hemolysis near an ultrasonically pulsating gas bubble, *Science* 169 (1970) 869–871.
- [62] P. Marmottant, S. Hilgenfeldt, Controlled vesicle deformation and lysis by single oscillating bubbles, *Nature* 423 (2003) 153–156.
- [63] X. Liu, J. Li, L. Zhang, X. Huang, U. Farooq, N. Pang, W. Zhou, L. Qi, L. Xu, L. Niu, et al., Cell lysis based on an oscillating microbubble array, *Micromachines* 11 (2020) e0288.
- [64] A. Hashmi, G. Yu, M. Reilly-Collette, G. Heiman, J. Xu, Oscillating bubbles: a versatile tool for lab on a chip applications, *Lab Chip* 12 (2012) 4216–4227.
- [65] H. Jeon, K.A. Mirgissa, S. Baek, K. Rhee, D. Kim, Excitation-frequency determination based on electromechanical impedance spectroscopy for a laser-microfabricated cavitation microstreaming micromixer, *Sens. Actuators A Phys.* 326 (2021), e112730.
- [66] C. Chu, B. Jiang, L. Zhu, F. Jiang, A process analysis for microchannel deformation and bonding strength by in-mold bonding of microfluidic chips, *J. Polym. Eng.* 35 (2015) 267–275.
- [67] C.-W. Tsao, D.L. DeVoe, Bonding of thermoplastic polymer microfluidics, *Microfluid. Nanofluid.* 6 (2009) 1–16.
- [68] A.M.D. Wan, T.A. Moore, E.W.K. Young, Solvent bonding for fabrication of PMMA and COP microfluidic devices, *J. Vis. Exp.* 119 (2017), e55175.
- [69] S. Prakash, S. Kumar, Fabrication of microchannels on transparent PMMA using CO<sub>2</sub> laser (10.6 μm) for microfluidic applications: an experimental investigation, *Int. J. Precis. Eng. Manuf.* 16 (2015) 361–366.
- [70] C. Matellan, A.E. del Río Hernández, Cost-effective rapid prototyping and assembly of poly(methyl methacrylate) microfluidic devices, *Sci. Rep.* 8 (2018) e6971.
- [71] A. Liga, J.A.S. Morton, M. Kersaudy-Kerhoas, Safe and cost-effective rapid-prototyping of multilayer PMMA microfluidic devices, *Microfluid. Nanofluid.* 20 (2016) e164.
- [72] Y.M. Lo, K.C. Chan, Introduction to the polymerase chain reaction, *Methods Mol. Biol.* 336 (2006) 1–10.
- [73] A. Marin, M. Rossi, B. Rallabandi, C. Wang, S. Hilgenfeldt, C.J. Kähler, Three-dimensional phenomena in microbubble acoustic streaming, *Phys. Rev. Appl.* 3 (2015), e041001.
- [74] I.R.G. Ogilvie, V.J. Sieben, C.F.A. Floquet, R. Zmijan, M.C. Mowlem, H. Morgan, Reduction of surface roughness for optical quality microfluidic devices in PMMA and COC, *J. Micromech. Microeng.* 20 (2010), e065016.
- [75] X. Dong, T. Yuan, M. Hu, H. Shekhani, Y. Maida, T. Tou, K. Uchino, Driving frequency optimization of a piezoelectric transducer and the power supply development, *Rev. Sci. Instrum.* 87 (2016), e105003.
- [76] B.H. Park, S.J. Oh, J.H. Jung, G. Choi, J.H. Seo, D.H. Kim, E.Y. Lee, T.S. Seo, An integrated rotary microfluidic system with DNA extraction, loop-mediated isothermal amplification, and lateral flow strip based detection for point-of-care pathogen diagnostics, *Biosens. Bioelectron.* 91 (2017) 334–340.
- [77] K.A. Melzak, C.S. Sherwood, R.F.B. Turner, C.A. Haynes, Driving forces for DNA adsorption to silica in perchlorate solutions, *J. Colloid Interface Sci.* 181 (1996) 635–644.
- [78] N.D. Olson, J.B. Morrow, DNA extract characterization process for microbial detection methods development and validation, *BMC Res. Notes* 5 (2012) 668.
- [79] R. Kant, A. Gupta, S. Bhattacharya, Studies on CO<sub>2</sub> laser micromachining on PMMA to fabricate micro channel for microfluidic applications, in: S.N. Joshi, U. S. Dixit (Eds.), *Lasers Based Manufacturing: 5th International and 26th All India Manufacturing Technology, Design and Research Conference, AIMTRD 2014*, 2015, pp. 221–238. Springer India, New Delhi.
- [80] J. Powell, Cutting non-metals, in: J. Powell (Ed.), *CO<sub>2</sub> Laser Cutting*, Springer, London, London, 1998, pp. 91–115.

- [81] E.V. Antonakou, D.S. Achilias, Recent advances in polycarbonate recycling: a review of degradation methods and their mechanisms, *Waste Biomass Valorization* 4 (2013) 9–21.
- [82] J. Jiang, J. Zhan, W. Yue, M. Yang, C. Yi, C.-W. Li, A single low-cost microfabrication approach for polymethylmethacrylate, polystyrene, polycarbonate and polysulfone based microdevices, *RSC Adv.* 5 (2015) 36036–36043.
- [83] H.A. Eltawahni, A.G. Olabi, K.Y. Benyounis, Effect of process parameters and optimization of CO<sub>2</sub> laser cutting of ultra high-performance polyethylene, *Mater. Des.* 31 (2010) 4029–4038.
- [84] K.F. Tamrin, Y. Nukman, I.A. Choudhury, S. Shirley, Multiple-objective optimization in precision laser cutting of different thermoplastics, *Opt. Lasers Eng.* 67 (2015) 57–65.
- [85] Y.-J. Chan, T.-H. Yuan, H.-C. Sun, T.-C. Lin, Characterization and exposure assessment of odor emissions from laser cutting of plastics in the optical film industry, *Aerosol Air Qual. Res.* 16 (2016) 2216–2226.
- [86] Y. Chan, T.-H. Yuan, Y.-H. Tsai, T. Lin, Characterization of endocrine disruptors and particulate matter emissions from laser cutting of plastic film in the tft-lcd industry, *Aerosol Air Qual. Res.* 17 (2017) 1539–1549.
- [87] Promega, Genomic DNA Extraction Kits, 2021. <http://www.Promega.Kr/en/products/nucleic-acid-extraction/genomic-dna/genomic-dna-extraction-kits/>.
- [88] Qiagen, MagAttract HMW DNA Handbook, 2020.
- [89] BioVision, Cell & Tissue Genomic DNA Extraction Kit, 2021. <http://www.Biovision.Com/documentation/datasheets/k1442.Pdf>.
- [90] Labgene Scientific, MagFast384 Universal Purification Kit, 2021. <http://www.Labgene.Ch/ideal-kits/600-magfast-universal-purification-kit.html>.
- [91] B. Zhou, S.S. Ho, S.U. Greer, X. Zhu, J.M. Bell, J.G. Arthur, N. Spies, X. Zhang, S. Byeon, R. Pattni, et al., Comprehensive, integrated, and phased whole-genome analysis of the primary encode cell line k562, *Genome Res.* 29 (2019) 472–484.
- [92] M. Jongen-Lavrencic, S. Saless, R. Delwel, C.M. Verfaillie, Bcr/abl-mediated downregulation of genes implicated in cell adhesion and motility leads to impaired migration toward ccr7 ligands ccl19 and ccl21 in primary bcr/abl-positive cells, *Leukemia* 19 (2005) 373–380.
- [93] J. Dumont, D. Euwart, B. Mei, S. Estes, R. Kshirsagar, Human cell lines for biopharmaceutical manufacturing: history, status, and future perspectives, *Crit. Rev. Biotechnol.* 36 (2016) 1110–1122.
- [94] E. Klein, F. Vánky, H. Ben-Bassat, H. Neumann, P. Ralph, J. Zeuthen, A. Polliack, Properties of the k562 cell line, derived from a patient with chronic myeloid leukemia, *Int. J. Cancer* 18 (1976) 421–431.
- [95] A. Maccani, W. Ernst, R. Grabherr, Whole genome sequencing improves estimation of nuclear DNA content of chinese hamster ovary cells, *Cytometry A.* 83 (2013) 893–895.
- [96] T.F. Scherr, C.F. Markwalter, W.S. Bauer, D. Gasperino, D.W. Wright, F. R. Haselton, Application of mass transfer theory to biomarker capture by surface functionalized magnetic beads in microcentrifuge tubes, *Adv. Colloid Interface Sci.* 246 (2017) 275–288.
- [97] P. Tho, R. Manasseh, A. Ooi, Cavitation microstreaming patterns in single and multiple bubble systems, *J. Fluid Mech.* 576 (2007) 191–233.
- [98] M. Long, M.A. Sprague, A.A. Grimes, B.D. Rich, M. Khine, A simple three-dimensional vortex micromixer, *Appl. Phys. Lett.* 94 (2009), e133501.
- [99] J.J. Benítez, J. Topolancik, H.C. Tian, C.B. Wallin, D.R. Latulippe, K. Szeto, P. J. Murphy, B.R. Cipriany, S.L. Levy, P.D. Soloway, et al., Microfluidic extraction, stretching and analysis of human chromosomal DNA from single cells, *Lab Chip* 12 (2012) 4848–4854.
- [100] R.S. Tuma, M.P. Beaudet, X. Jin, L.J. Jones, C.-Y. Cheung, S. Yue, V.L. Singer, Characterization of SYBR gold nucleic acid gel stain: a dye optimized for use with 300-nm ultraviolet transilluminators, *Anal. Biochem.* 268 (1999) 278–288.
- [101] A.K. Jahromi, M. Saadatmand, M. Eghbal, L.P. Yeganeh, Development of simple and efficient lab-on-a-disc platforms for automated chemical cell lysis, *Sci. Rep.* 10 (2020), e11039.
- [102] A. Osei-Bimpong, R. McLean, E. Bhonda, S.M. Lewis, The use of the white cell count and haemoglobin in combination as an effective screen to predict the normality of the full blood count, *Int. J. Lab. Hematol.* 34 (2012) 91–97.
- [103] E. Menu, C. Mary, I. Toga, D. Raoult, S. Ranque, F. Bittar, Evaluation of two DNA extraction methods for the PCR-based detection of eukaryotic enteric pathogens in fecal samples, *BMC Res. Notes* 11 (2018) 206.
- [104] P. Amicucci, M. Gennarelli, G. Novelli, B. Dallapiccola, Prenatal diagnosis of myotonic dystrophy using fetal DNA obtained from maternal plasma, *Clin. Chem.* 46 (2000) 301–302.

**Abdi Mirgissa Kaba** is a Ph.D. student in the Department of Mechanical Engineering at Myongji University. He received his B.S. and M.S. degrees in Mechanical Engineering from Addis Ababa University, Ethiopia in 2015 and 2017 respectively. His research interest includes microfluidics, optimization of polymer-based microfabrication processes, and microfluidic lab-on-a-chip devices for biomolecular analysis.

**Hyunjin Jeon** is an assistant engineer at Inventage Lab and a Master's student in the Department of Mechanical Engineering at Myongji University, South Korea. She is expected to receive her degree in 2021. Her research interest includes lab-on-a-chip, laser microfabrication, and ultrasonic actuation.

**Areum Park** is a manager at the Department of Research and Development in Biomedex. She received her B.S. and M.S. degrees in NanoBio Engineering from Inje University, South Korea in 2009 and 2011 respectively. Before starting her managerial work at Biomedex, she worked as a researcher in the Department of Research and Development at Biomedlab, Seoul and LabGenomics, Seongnam for 4 years. Her research interest focuses on molecular diagnostics.

**Kyungjin Yi** is a researcher in the Department of Research and Development at Biomedex. She received her B.S. degree in Bioscience from Suwon University, South Korea in 2011. Before starting her work at Biomedex, she worked as a researcher in the Institute of Gastroenterology in the College of Medicine at Yonsei University for 4 years. Her research interest focuses on molecular diagnostics.

**Seonhyeok Baek** is a Master's student in the Department of Mechanical Engineering at Myongji University, South Korea, and is expected to receive his degree in 2022. His research interest includes microfluidics, laser microfabrication, and MEMS (Micro-Electro-Mechanical-Systems) electrolytic actuators.

**Aeja Park** is the CEO of Biomedex and an emeritus professor in the College of Medicine at Chung-Ang University, South Korea. She received her B.S. degree in Medical Science from Ewha University in 1976. She received her M.S. and Ph.D. degrees in Laboratory Medicine from Yonsei University, South Korea in 1980 and 1983, respectively. Her research interest focuses on molecular diagnostics.

**Dohyun Kim** is an associate professor in the Department of Mechanical Engineering at Myongji University, South Korea. He received a B.S. and M.S. degrees in Mechanical Engineering from Sogang University, South Korea in 1993 and 2001, respectively. He graduated from the University of California, Los Angeles, United States in 2008 with a Ph. D. degree in Electrical Engineering. Before starting his professorship at Myongji University, he worked as a postdoctoral scholar in the Bioengineering Department at the University of California, Berkeley for 3 years. His research interest includes polymer microfabrication, MEMS actuators, and microscale bioanalytical systems for disease diagnostics.